4-5-2023

Numerical Flume for Wave Dissipation by Mangrove Prop Roots

Rebecca L. Schurr
Louisiana State University and Agricultural and Mechanical College

NUMERICAL FLUME FOR WAVE DISSIPATION BY MANGROVE PROP ROOTS

A Thesis

Submitted to the Graduate Faculty of the
Louisiana State University and
Agricultural and Mechanical College
in partial fulfillment of the
requirements for the degree of
Master's in Coastal and Ecological Engineering

in

The Department of Civil and Environmental Engineering

by
Rebecca Leigh Schurr
B.S., University of Delaware, 2021
May 2023

Acknowledgments

First, I would like to thank Dr. Chris Kees, for advising me throughout the two years I've been at LSU as well as working on this project with me and taking the time to teach me various programming languages. I would also like to thank Dr. Clint Willson and Dr. Robert Twilley for making up my committee and providing valuable feedback.

I also want to extend my thanks to the team of post-docs and graduate students that have assisted me throughtout this journey. Wen-Huai Tsao for your advice and assistance on both the numerical flume and the PFT flume. Linoj Vijayan Nair Rugminiamma for your feedback on the numerical flume and it's components as well as both academic and professional advice. The rest of our group, Arnob Barua, Jin Ikeda, and Shabnam Mirheidarian, for your valuable feedback and support. I would also like to thank Elizabeth Bogan for your support and knowledge on mangroves and CAD as well as your friendship while at LSU.

To my parents, Coleen and Gary Schurr, and my sister, Emily Schurr, for your continued support and love throughout this entire process. As well as my grandparents for your support, phone calls, and love throughout my time at LSU. Finally, I'd like to thank my friends back in Pennsylvania for your encouragement and visits to Louisiana over these two years and all of the friends that I have made since coming to LSU.

Table of Contents

List of Tables

List of Figures

Abstract

Mangroves provide shorelines with many beneficial engineering services, including shoreline stabilization, wave attenuation, and damage mitigation during tsunami or tropical cyclone events. This research focuses on wave attenuation rates and drag coefficients, and how they are affected by mangrove prop roots. Previous lab research using a physical wave flume has quantified wave height decay and drag coefficients for synthetic mangrove forests and confirmed that attenuation does indeed increase as mangrove forest density increases. This research will use a 3D numerical flume model developed in Proteus, a Python package, to simulate prior physical model experiments. This work will attempt to validate the numerical flume output, specifically the wave height decay and drag coefficients it yields from an embedded discretization of the mangrove trunk geometry based on the Cut Finite Element Method. This research will then lay the groundwork for the more general approach of using the numerical flume to predict coefficients for real mangrove forests using geometry obtained from LiDAR scans or other site-specific geometric characterizations. The problem solved by this general approach is that wave attenuation and drag coefficients are functions not only of stem and prop root density but more generally of the morphology of the real mangrove system geometry. This varies across multiple scales (prop roots orientations to trunk distributions) and is, therefore, difficult to reproduce in a physical flume. This research supports the advancement of numerical wave flume modeling as an engineering tool for going beyond physical model studies to scenarios where a physical flume may not be available or practical. We show that the numerical wave flume accurately reproduces baseline wave transmission in the Oregon State flume experiments and both baseline and vegetated wave attenuation in the small flume at

Patrick F. Taylor Hall. This research can also provide the framework for a more accurate understanding of real-world mangrove forests and their effects on wave attenuation.

Chapter 1. Introduction

1.1. Problem Statement

Emergent vegetation like mangrove forests have been identified as possible features that could provide great benefits to coastal protection; however, much of the available data is limited to field studies and laboratory experiments. Results from various field studies led to physical laboratory experiments using idealized models of red mangroves (*Rhizophora mangle*). Due to the species' complex trunk-prop root system, experiments have used a variety of different methods to model the prop roots [8]. Using the wave flume located in Patrick F. Taylor Hall (PFT), an idealized mangrove forest of polyvinyl chloride (PVC) pipe trunks was used to simulate the mangrove trunks' effects on wave attenuation. This experiment was done using the 6.08 m Wave Flume (WF) in PFT. The bathymetry of the WF remained constant for a 4.9 m section followed by a 1.18 m 29.6% grade as the final beach slope as shown in Figure 1.1.

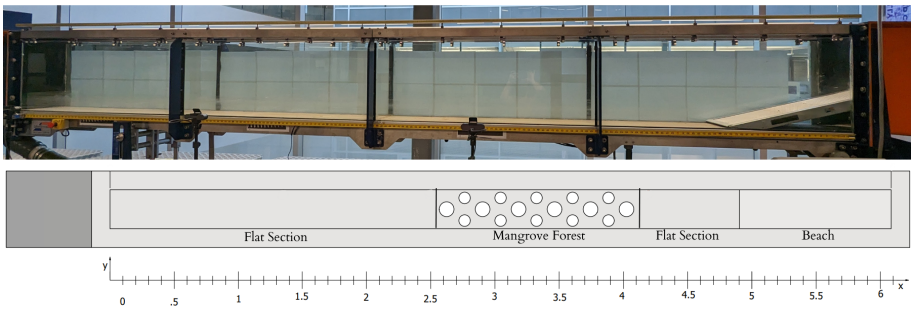

Figure 1.1. PFT Flume and schematic top-view configuration and layout

The experiment at PFT will calculate the wave height for each scenario and provide results for the validation of the numerical model. The validation of the numerical model using the same idealized structure of the mangrove forest is the first step before the eventual implementation of LiDAR scans within the model.

1.2. Research Objective

For this research, 2D (vertical) and 3D numerical flumes were created using Python based on the bathymetry of the PFT wave flume as well as the large flume at Oregon State University where prototype scale experiments with PVC prop root models were recently conducted [4]. During the course of this research it became apparent that a smaller and less complex experiment was needed for initial validation, so we adapted the PFT wave flume for that purpose. In the PFT flume, three mangrove layouts were used to demonstrate the effects of mangrove trunk density on wave attenuation; baseline (no forest), low-density, and high density. The forest densities were added to the numerical flume through the embedding of cylinders based on the CutFEM method with a mesh size slightly smaller than the radius of the trunk. The trunk dimensions were determined based on the available PVC pipes that would eventually be implemented into the PFT flume for a physical experiment to validate the numerical flume. Three varying wave conditions for regular wave cases were also chosen. This provided a variety of results for the regular wave case. Following the running of the nine simulations, the wave decay rates and drag coefficients were calculated, and the trends were compared to the previous physical experiments.

Overall, the objectives of this research were:

- to create a 3D numerical flume using Python with an embedded mangrove forest using the CutFEM approach;
- to calculate the wave height decay rates and drag coefficients produced by the two trials and three layouts for multiple mesh sizes for physical and computational models;

- and, finally, to compare the numerical results to the physical experiment and evaluate the accuracy of the computational flume for calculating wave height decay and drag coefficients.

Chapter 2. Literature Review

2.1. Theoretical Background

Theoretical equations that quantified the effects of emergent vegetation on wave attenuation were first proposed in a panel report for National Research Council of the National Academy of Sciences [9]. These equations connected vegetation-specific drag coefficients to the wave attenuation rates but assumed emergent vegetation conditions (vegetation taller than waves) and linear wave theory. In addition, the equation assumed the drag was constant over the depth of vegetation. The equation from [9] is

$$\frac{H_t}{H_i} = \frac{1}{[1 + \frac{C_D H_i d D w}{3\pi(b^2 h^2)}]} \tag{2.1}$$

where the left-hand side is the transmission coefficient (transmitted wave height, H_t, divided by incident wave height, H_i), C_D is the drag coefficient, d is the mean wetted height of vegetation, D is the vegetation effective mean diameter, w is the width of the vegetation patch, b is the mean horizontal spacing of the vegetation based on their center locations, and h is the mean vegetation water depth.

These equations were later expanded upon to consider both an arbitrary water depth and arbitrary tree height [10]. This produced the extended equation for the wave transmission coefficient based on cross-shore distance of vegetation and wave attenuation coefficient noted as

$$\frac{H_t}{H_i} = \frac{1}{1 + \alpha x} \tag{2.2}$$

where

$$\alpha = \frac{4 A_{t,m} N H_i C_D k}{9\pi} \frac{\sinh^3(kd) + 3\sinh(kd)}{\sinh(kh)(\sinh(2kh) + 2kh)} \tag{2.3}$$

where α is the wave height decay coefficient, $A_{t,m}$ is the mean projected area per unit

height per tree, N is the number of trees per unit area, k is the wave number ($2\pi/L$), and L is the wavelength.

However, the equations were still limited by only using regular waves until it was developed further to include random waves [11]. In the random wave formulation, the transmission coefficient is defined as the ration of the transmitted and reflected root-mean-square wave height under the assumption of a Rayleigh distribution for a narrow-banded wave spectrum described by the peak period and root-mean-square wave height. This equation is given as

$$\frac{H_{rms,t}}{H_{rms,i}} = \frac{1}{1+\tilde{\alpha}x} \tag{2.4}$$

where

$$\tilde{\alpha} = \frac{4A_{t,m}NH_{rms,i}C_Dk}{3\sqrt{\pi}} \frac{\sinh^3(kd)+3\sinh(kd)}{\sinh(kh)(\sinh(2kh)+2kh)} \tag{2.5}$$

where H_{rms} denotes the root mean square wave height, and $\tilde{\alpha}$ is the wave height decay coefficient for random waves. It was these two equations, 2.2 and 2.5, that provided the framework for the OSU experiment [12] which focused on both regular and random wave scenarios.

2.2. Laboratory Studies

The OSU Large Wave Flume (LWF) was not the first laboratory experiment to use artificial mangrove trunk-root systems in an effort to measure this complex system's effect on wave attenuation but previous experiments used different materials in the creation of their idealized forests. These earlier studies focused on the wave attenuation effects of mangroves through the creation of various idealized forests within their flumes. One previous experiment considered the interaction of unidirectional flow with a 1:7.5 scale model in

order to estimate the turbulent kinetic energy and drag coefficients [1]. Their model consisted of larger diameter aluminum cylinders for the trunk and then smaller diameter rods for the roots as well as bending the model roots to resemble the curvature of the measured prop roots based on a mangrove forest in Berlayer Creek, Singapore. They determined that their model produced measured drag coefficients that were consistent with values reported in previous field studies [1].

Another previous study used acrylic tubes for the trunk and brass rods for the roots and constructed a 1:12 scale forest [2]. Their goal was similar in that they also wanted to study turbulent kinetic energy and drag coefficient for unidirectional flow. However, the estimation of projected area created a quantified uncertainty in the drag coefficients. A third laboratory experiment investigated wave attenuation and drag forces for both random and regular waves [3]. This experiment used PVC pipe as the mangrove trunk and aluminum rods for the roots of the model tree at a 1:6-scale. All three laboratory experiments used the Reynolds number to determine the drag coefficients using the depth-averaged velocity and equivalent mean diameter. The most recently completed experiment used an idealized prototype scale physical model [12]. This experiment concluded that changing the mangrove forest density had a direct effect on wave attenuation and that drag coefficients were Reynolds number dependent [12]. This compared well to previous reduced scale models. The overall design of the artificial mangroves did remain the same throughout the experiments as displayed in Figure 2.1.

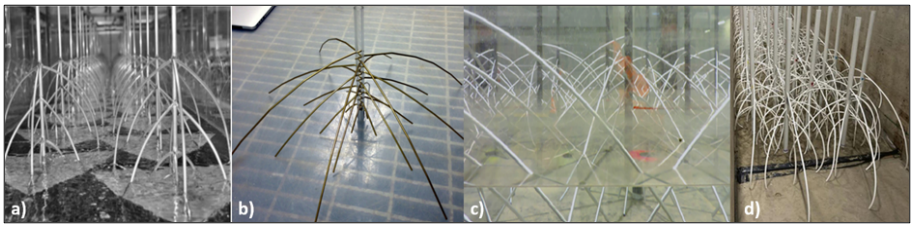

Figure 2.1. Artificial mangrove trunk-root systems. Source: a) Zhang et al. [1], b) Maza et al. [2], c) Maza et al. [3], d) Kelty et al. [4]

These recent laboratory experiments at OSU investigated thirty-six different scenarios each comprising of three different mangrove forest conditions: no forest, a low-density forest, and a high-density forest [4]. Random and regular wave conditions were both considered at varying wave periods and submerged vegetation heights in an effort to quantify the effect of the forest density on wave attenuation based on differing scenarios. To change the mangrove forest density from high to low, the layout of the forest was also changed. The forest went from a high-density (HD) case where the specimens were positioned in a staggered arrangement to a low-density (LD) case where the mangroves were selected for removal such that the number of specimens in each 3.66 m by 3.66 m section was reduced from ten to five and each cross-shore row had a total of five trees [4]. This procedure resulted in a non-uniform positioning of specimens for the low-density configuration. These configurations are shown in Figure 2.2. It was concluded that increasing the mangrove forest density by a factor of two increased the wave decay coefficient by a factor of 2.0, on average for the random wave conditions, and by 2.2 for regular wave conditions, as well as the drag coefficients being Reynolds number dependent [4]. These conclusions were based on Equations 2.2 and 2.5. It was also determined that wave height decay was not affected by a grid or random mangrove layout, but rather by the density variation [4]. However, the physical model was only able to look at two density cases for each scenario.

The numerical model will allow for varying mangrove forest densities to be tested following it's validation based on a similar experiment run at PFT.

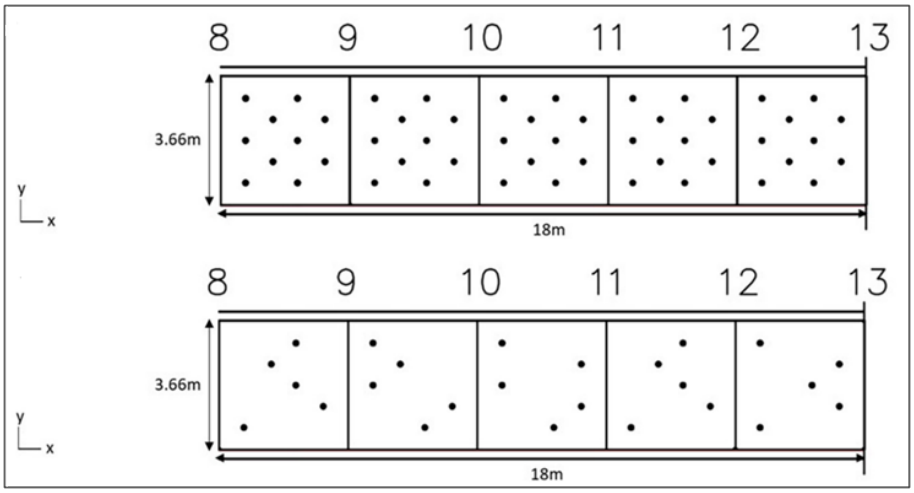

Figure 2.2. High-Density Forest Configuration and Low-Density Forest Configuration [4]

2.3. Numerical Methods

Many methods have been previously developed for embedding solid obstacles in viscous incompressible flows within numerical models. In this work we solve the multi-phase Navier-Stokes (NS) equations for a two-fluid (air/water) field with a potentially very complex solid object embedded. The main numerical difficulty is the eventual complexity of the solid obstacle's surface and its potential motion when the obstacle is vegetation. Prop roots pose a particular challenge due to their tangled structure, wide range of stem scales, and ultimately that the source of the geometric description is LIDAR. In this work we represent it as an implicit surface (signed distance field). The challenge is then to enforce no-slip boundary condition with comparable accuracy to the boundary-conforming Finite Element Methods (FEMs) that have proved successful in aerospace, mechanical, and naval architecture applications, where boundary-conforming meshes are easier to generate for man-made geometries. Notable early work by Hansbo and Hansbo applied Nitsche's

penalty-based approach to enforce Dirichlet boundary conditions on the cut cells of immersed boundary problems [5]. The standard Finite Element (FE) basis is replaced by changing each standard basis function living on an element that intersects the interface by two new basis functions, namely its restrictions to Ω_1 and Ω_2, respectively. Ω_1 and Ω_2 are two open sets located within Ω which is a bounded domain in $\mathbb{R}^2$ with a convex polygonal boundary $\partial\Omega$ and an internal smooth boundary Γ. However, the new basis functions still use the same nodes as the original triangulation–not new nodes conforming to the embedded interface. Triangles intersected by the interface surface, Γ, use a combinations of old nodes from the original mesh and newly duplicated nodes as shown in Figure 2.3. Hansbo and Hansbo emphasize that the new nodes are convenient support points for the definition of a continuous, piecewise linear, approximation rather than nodes in the standard finite element sense.

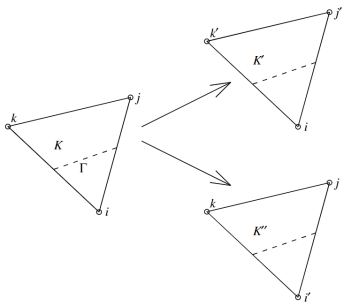

Figure 2.3. The split of a triangle with method proposed by Hansbo and Hansbo [5]

This basic method was then extended and improved to a wide range of scenarios and augmented with stabilization and precise stability and error estimates [6]. This method, known as the Cut Finite Element Method (CutFEM), enforces boundary conditions or jump condition on an implicit surface (e.g. signed distance function) on the background grid. The background grid is then used to represent the approximate solution of

the governing partial differential equations (PDEs). CutFEM is then able to build on a general finite element formulation for the approximation of PDEs, in both the bulk and on surfaces that can handle elements of complex shape, and where boundary and interface conditions are built into the discrete formulation. Using Nitsche's approach to stabilize the Stokes' problem, CutFEM is able to calculate both pressure approximation and the computed velocity as shown in Figure 2.4. Most importantly, it does so with accuracy and stability comparable to boundary-conforming methods. Compared to previous classical computational methods, the CutFEM "cuts" meshes to fit the solid interfaces that do not conform to the mesh.

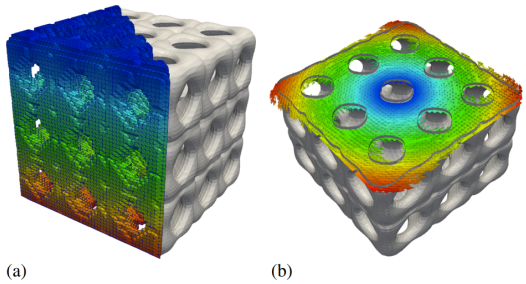

Figure 2.4. Stokes flow in (a) Pressure approximation and (b) Velocity approximation in a cross-section through the xy-plane from [6]

A frequent criticism of CutFEM methods is that they are extremely complex to implement, requiring extraction of cut cells and interfaces and use of special finite elment assembly algorithms. Kees extended a high-order CutFEM method for incompressible flow applications with embedded interfaces with a simplified finite element assembly based on representing generalized Dirac and Heavisde functions with so-called equivalent polynomials to calculate the cut cell integrals without actually forming the cut cells [7]. The original approach applied to moving solid obstacles within a containing incompressible fluid phase, Figure 2.5. This allowed for the combination of CutFEM and equivalent polyno-

mials that conserves momentum between both the fluid and solid due to the use of the discrete numerical momentum flux from Nitsche's method for enforcement of the no-slip condition of the solid. This research was able to create a method that is robust, accurate, and efficient for upgrading FEM codes to include embedded boundaries with CutFEM [7]. This approach and implementation was used for the current study, but it required extensions for the two-phase Reynolds' Averaged Navier-Stokes model for air-water flows to model water wave interaction with the mangroves. The air-water interface was modeled with existing conservative level set methods extended to include embedded solid boundaries and some details of the extension are the subject of on-going development and a future journal article.

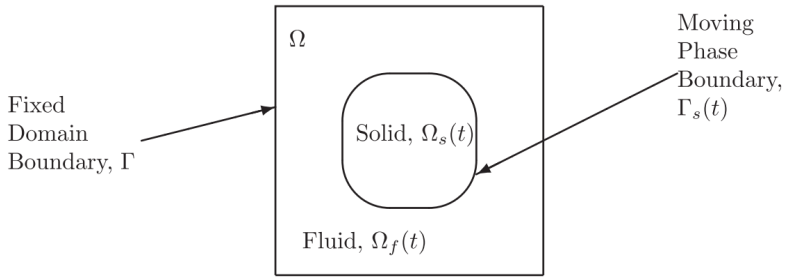

Figure 2.5. The fixed computational domain and boundary, with two dynamic subdomains and phase boundary to determine the signed distance function from [7]

Chapter 3. OSU Numerical Flume

The OSU experiment previously mentioned in Section 2.2 was the initial target for validating the numerical flume. For increased accuracy in the random waves that were used in the physical flume, we used the time series analysis method to reproduce a close approximation to the physical incident wave gauge time series [13]. The results from the first wave gauge at OSU for each trial was collected and stored as a .csv file [14]. The time series class takes the .csv file with the wave elevations and time from the first wave gauge and replicates it to produce a similar, ideally exact, wave output in the code. Figure 3.1 shows the results of the time series class when compared to the results from the physical LWF in 2D for case TI-HV3-3 [4]. These wave gauge results showed improved accuracy in creating the same output as the physical flume.

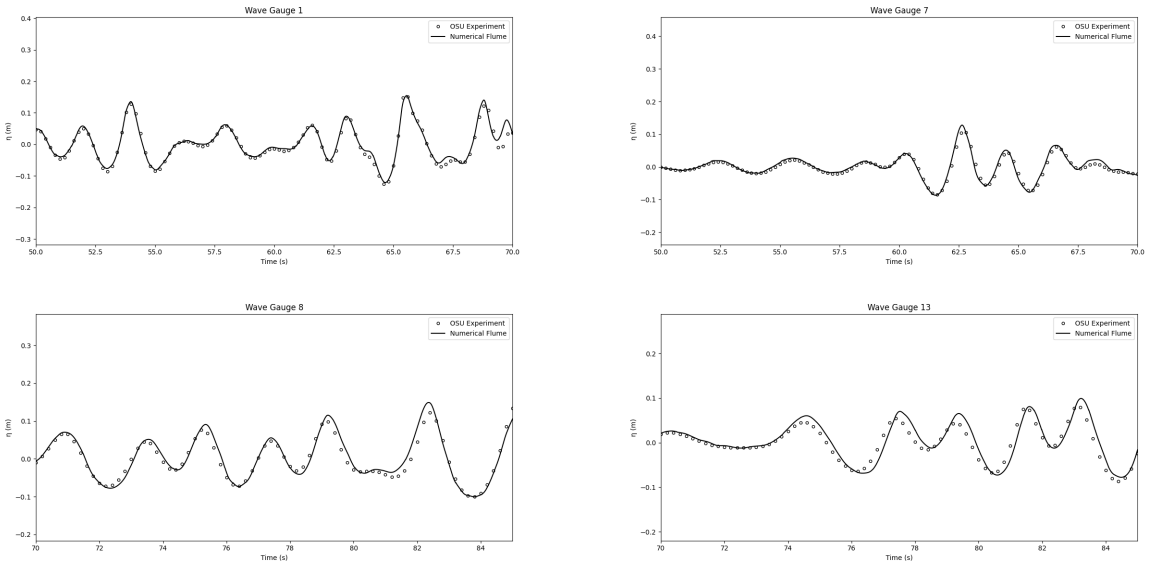

Figure 3.1. TimeSeries Class WG Results from OSU Experiment and Numerical Flume for 2D Case

While Figure 3.1 only shows the results for one case, case TI-HV3-3 had the most difficult set of wave characteristics to reproduce and the time series class was able to suc-

cessfully reproduce them. There were also other trials from Kelty et al. run with simpler wave characteristics and these produced results with similar accuracy to case TI-HV3-3 [4]. Overall, time series is the best method in wave making for validation of the OSU physical flume.

Following the validation of the 2D cases we began attempting the 3D version of the flume to be used with the embedded mangrove models. The width was first increased by one mesh element to make sure accuracy with the time series class was still in place with this added dimension. As we began to assess computational needs for the full 3D cases, we decided to post-pone validation on the OSU model until a simpler and less computationally intensive validation study on the PFT flume could be completed. This simpler flume is used for the remainder of this thesis.

Chapter 4. PFT Physical Flume Experiment

The PFT flume was implemented for both a physical and numerical experiment. The flume has a total length of 6.08 m with a constant 4.9 m section followed by a 1.18 m 29.6% grade as the beach slope with a constant width of 0.3 m and height of 0.45 m. The beach slope was a permeable surface with the purpose of absorbing the incoming wave and reducing reflected waves. The wave maker is a flap-type with the bottom of the paddle fixed by a rubber hinge and the top connected to a servo motor with a brass rod. Two wave conditions were tested for each of the three mangrove forest layouts. The mangrove forest was created with both 4in and 3in PVC pipes similar to the Kelty et al. experiment [4].

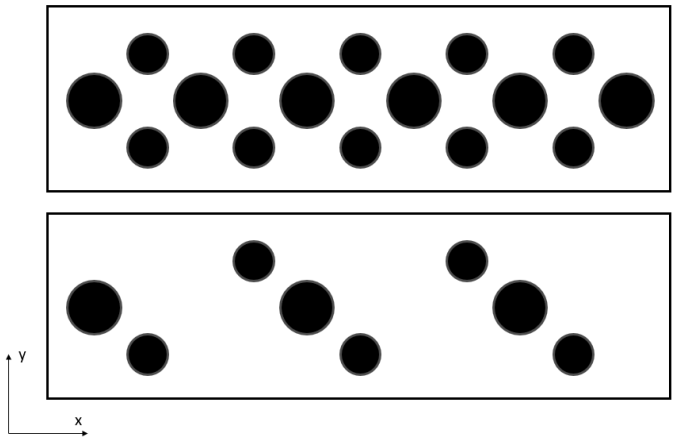

Figure 4.1. Numerical Flume High-Density Forest Configuration and Low-Density Forest Configuration

The PFT wave flume is unable to create waves based on specific values for amplitude and frequency. Due to this, the first wave condition was a high amplitude and low frequency and the second condition was a low amplitude and high frequency. The first condition was run for all layouts before being adjusted to the second condition. The waves were recorded from three cameras located at 1.35 m, 2.49 m, and 4.19 m which was after

the wave maker, prior to the forest, and after the forest, respectively. Figure 4.2 shows the final two cameras encircled in a green circle. These cameras are able to capture video of the free-surface motion due to the water being dyed light red.

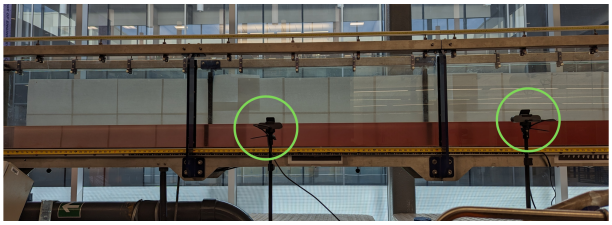

Figure 4.2. PFT Physical Wave Flume with final 2 cameras circled

The cameras are able to record data at a sampling rate of the camera is 60 Hz. The camera records HD video (1920x1080), which results in a resolution of about 0.3 mm/pixel. The image is analyzed by 'canny' function in MATLAB to find edges in 2-D grayscale image. This then allowed for the determination of the wave heights and water depth for each of the six trials. Table 4.1 shows the calculated wave heights at each of the three camera locations as well as the time period based on the calculated frequency. However, the PFT wave flume does have a slight leak in it and that is evident in the changing MWL as the simulations continued running. The attenuation and drag coefficient results from the physical experiment will be further discussed in Chapter 7.

Table 4.1. PFT Experimental Results

Trial	Layout	MWL (m)	H_1 (m)	H_2 (m)	H_3 (m)	T (s)
Wave-1	BL	0.132	0.0386	0.0365	0.0427	1.32
Wave-1	LD	0.134	0.0443	0.0452	0.0426	1.32
Wave-1	HD	0.138	0.045	0.0419	0.0393	1.32
Wave-2	BL	0.128	0.0338	0.0324	0.0324	0.74
Wave-2	LD	0.125	0.0303	0.0652	0.0178	0.74
Wave-2	HD	0.12	0.0344	0.0324	0.0175	0.74

Chapter 5. Experimental Setup

5.1. Numerical Flume

The numerical flume was created with Proteus. Proteus is an open-source toolkit for Python that consists of various modules that can be used within Python code. For this research the WaveTools, SpatialTools, and TwoPhaseFlow modules are vital. SpatialTools was used to create the wave flume based on the exact bathymetry of the PFT wave flume (WF). The bathymetry of the WF remained constant for a 4.9 m section followed by a 1.18 m 29.6% grade as the final beach slope with a constant width of 0.3 m.

To create the flume, a series of vertices were determined based on significant points in the cross-shore direction. Significant points to match the bathymetry included the wave generation zone, the mangrove forest, and the beach slope at the end of the flume. Once the coordinates of these locations were determined, they were then connected via segments and given a classification if the segments were solid, fluid, etc. Following the creation of the 3D flume, an array of mangrove trunks was created as a signed distance field and embedded using CutFEM with equivalent polynomials [7]. The water at the mean water level can be seen in Figure 5.1 as the blue colored area, the open flume area is noted in grey, the black area is the wave generation zone, and the red outline notes the location of the mangrove forest. The mangrove forest will be discussed later in Section 5.3.

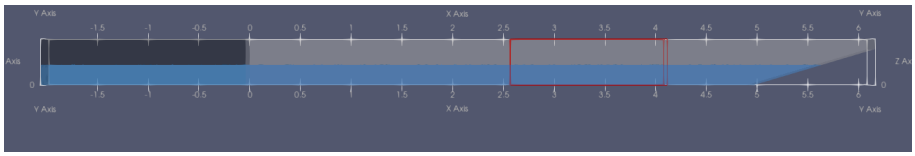

Figure 5.1. 3D Numerical Wave Flume visualized in Paraview

5.2. Instrumentation

The PFT wave flume uses a combination of three cameras and MATLAB code to calculate the wave heights. Calculations occurred prior to the forest, within the mangrove forest, and following the forest. In Figure 5.2, the three camera locations are denoted by the red pillars.

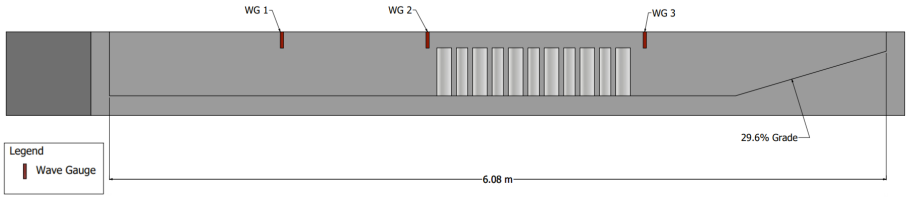

Figure 5.2. Overview of instrument placement in the PFT Large Wave Flume

In Figure 5.2, the most seaward (WG 1) and landward (WG 3) wave gauges are shown with the first wave gauge (WG1) placed at x=1.35 m to measure the incident waves and the last gauge (WG3) is installed at x=4.19 m prior to the beach slope. The second wave gauge is installed within the forest at x=2.49 m. The wave gauges in the numerical flume calculated the volume of fluid based on a line integral and therefore, required a minimum z-coordinate and maximum z-coordinate.

Table 5.1. Coordinates for wave gauges (WG) from Numerical Flume

	Numerical Coordinates			
Instrument Name	x (m)	y (m)	z-min (m)	z-max (m)
WG 1	1.35	0.15	0.0	0.45
WG 2	2.49	0.15	0.0	0.45
WG 3	4.19	0.15	0.0	0.45

5.3. Mangrove Forest

This research used three layouts comprised of a baseline (BL) layout without the mangrove forest, a low-density forest and a high-density forest. The low-density (LD) for-

est consisted of 8 trees whereas the high-density (HD) forest had 16. The mangrove forest trunks also consisted of two different radii. The smaller trunks had a radius of 0.04445 m and were the outer rows of the forest, while the larger trunks had a 0.05715 m radius and were the center row. The overall layout of the mangrove forest was based on the layouts implemented by Kelty et al. [12] with the low density forest being half the amount of trees as the high density forest. The low density forest also kept the same ratio of large trunks to small trunks as the high density forest. A calculation was completed to determine the basal area for each mangrove forest layout. The basal area of the low-density and the high-density forests were 1227 m^2ha^{-1} and 2453 m^2ha^{-1}, respectively. When compared directly to the Atlantic East Pacific (AEP) and Indo-West Pacific (IWP) biogeographical region these results were notably larger than a real mangrove forest [15]. The AEP and IWP forests have a basal area of 19.37 $\pm$ 0.38 m^2ha^{-1} and 25.18 $\pm$ 0.45 m^2ha^{-1}, respectively [15]. Overall the basal area of the model mangrove forest is unrealistic when compared to real-world mangrove forests.

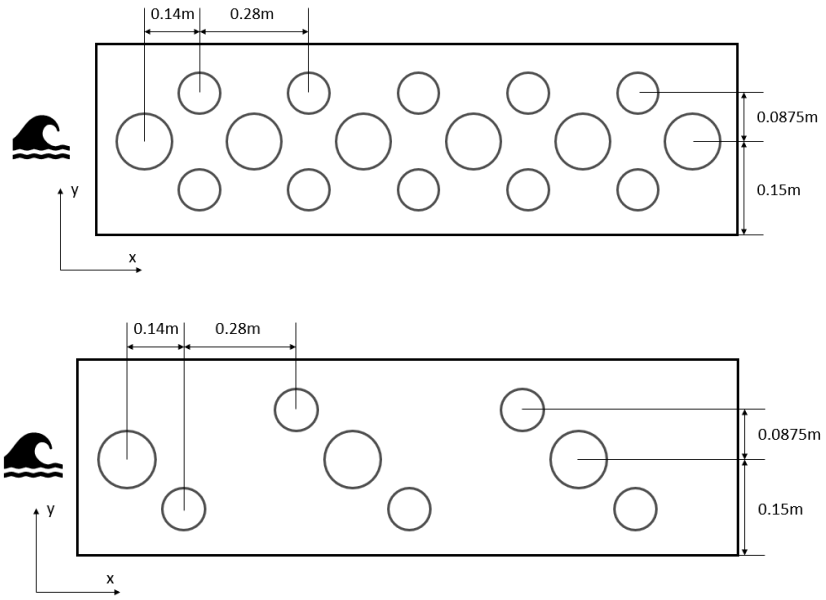

Figure 5.3. HD (upper) and LD (lower) Model tree spacing in each bay (Not to scale)

Using CutFEM, an embedded function was added to the flume that calculates the distance between the center of the trunk and a variable point within the domain mesh. This distance was then compared to the trunk's radius and any point inside the trunk was designated as a negative value; thus, creating a no flow-solid object. Whereas, any point outside of the trunk could proceed as before. The Paraview visualization of these layouts produced within the numerical flume is in AppendixA.

Chapter 6. Experimental Procedure

6.1. Wave Conditions

This research uses regular waves as that is what can be produced by the wave maker in the PFT flume. The target conditions for the regular wave conditions are in Table 6.1 and were determined by three parameters: still mean water level MWL, target wave height H, and wave period T. These conditions were determined from the experimental results from the PFT flume. While the wave period remained the same for all flume layouts, the wave height and still mean water level varied slightly.

Table 6.1. Target Wave Conditions for Regular Waves

Regular Wave Cases				
Trial	Layout	MWL (m)	H (m)	T (s)
TR-1	BL	0.132	0.039	1.32
TR-1	LD	0.134	0.044	1.32
TR-1	HD	0.138	0.045	1.32
TR-2	BL	0.128	0.034	0.74
TR-2	LD	0.125	0.030	0.74
TR-2	HD	0.12	0.034	0.74

As previously mentioned, the WaveTools module from Proteus was utilized to create the waves for the numerical flume. In the regular waves case, the monochromatic wave class used the Linear Wave Theory to create waves based on the parameters from Table 6.1.

6.2. Data Analysis

The numerical flume instrumentation included three wave gauges that provided the wave height at varying locations. Following the completion of all simulations, a quick check was done with all the gauges to see if the waves attenuated as they moved through

the mangrove forest when compared to all the layouts. Figure 6.1 shows the wave gauge 3 results for each layout for the first trial, but all the wave gauge data can be found in Appendices B and C for TR-1 and TR-2, respectively.

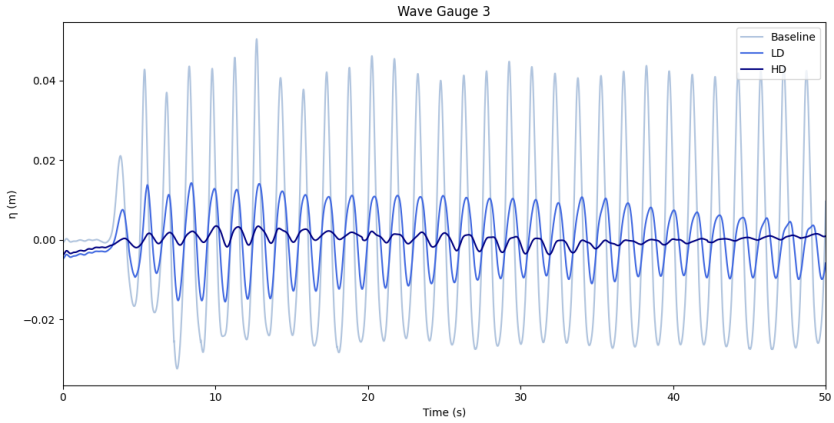

Figure 6.1. WG 3 Results for Numerical Flume for TR-1 for all cases

In order to use Equation 2.3, the mean projected area per unit height per tree, $A_{t,m}$, would need to also be determined. The mangrove forest section was divided into five and six different bays for the LD and HD layouts, respectively, as shown in Figure D.2 in Appendix D. The projected area for each bay, noted in Appendix D, was then divided by the number of trees in the bay. This value was then averaged overall to determine the mean projected area per unit height per tree, $A_{t,m}$, as used in Equation 2.3. Another method for finding the projected area involved calculating the actual projected area per tree per unit height, $A_{h,m}$, using the averaged, weighted diameter of the trees.

Table 6.2. Dimensional Values for Mangrove Tree Model

Layout	$A_{t,m}$ (m^2/m)	$A_{h,m}$ (m^2/m)
LD	0.093	0.098
HD	0.091	0.098

Chapter 7. Experimental Results

7.1. Wave Attenuation

The total spectral estimate of the significant wave height, H_s, for the wave gauges (WG) was determined using a script created in Python for both the physical and numerical flumes. In addition, there was a loss of water in the numerical flume upon the addition of the mangrove forests. This water loss was at a constant rate and was taken into account by detrending the data to keep the mean water level constant.

Figure 7.1 shows the results for the numerical flume TR-1 with the mesh diameter equal to 0.04 m for the detrended data of the LD and HD cases. The H_s values with respect to the x location are shown, origin of x-axis located at the wave maker, for the wave gauges of the HD (red), LD (yellow) and BL (blue) layouts.

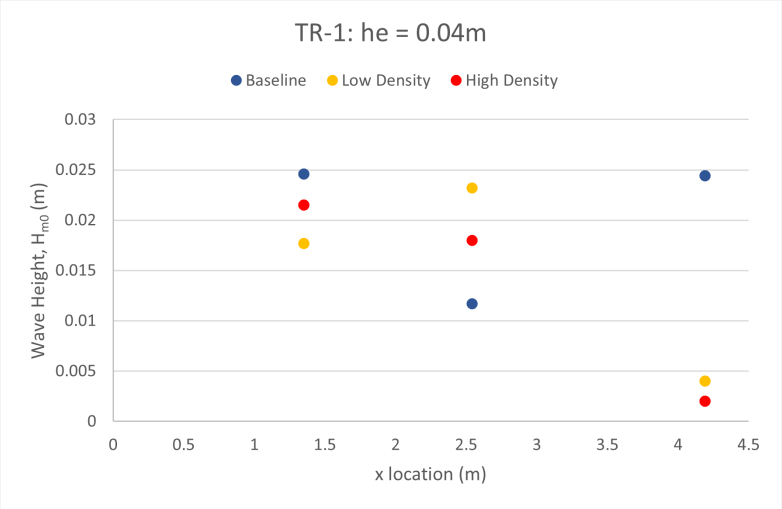

Figure 7.1. Total spectral estimate of the significant wave height, H_s, with respect to x location for wave gauges for TR-1 for he=0.04m

In Figure 7.1, the H_s values for the HD and LD layouts steadily decreased throughout the flume and there is also a slight decrease with the BL layout as well. overall, the HD layout had the greatest decay rate of H_s, followed by the LD layout. In order to de-

termine the wave height decay rate, the slope between WG1 and WG3 was calculated for each layout and this is represented by the dotted lines in Figure 7.2.

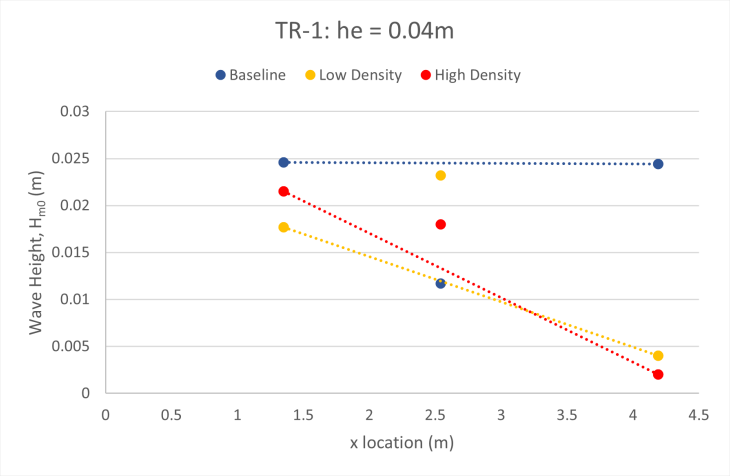

Figure 7.2. Total spectral estimate of the significant wave height, H_s, and linear line of best fit for each layout for TR-1 for he=0.04m

A statistical analysis was also completed on the wave height data. The purpose of this analysis was to determine if the calculated wave attenuation could simply the result of wave height variations in the flume. Since the standard deviation of the wave height variation was an order of magnitude smaller than the calculated wave attenuation for cases with mangroves, we deeded the measured attenuation by the mangrove models significant.

Table 7.1. Table of significant wave heights, H_s, and standard deviation, σ

Trial	Mangrove Case	Mesh Size, he (m)	$H_{s,1}$ (m)	$H_{s,3}$ (m)	$H_{s,1} - H_{s,3}$ (m)	σ_1 (m)	σ_3 (m)
TR-1	BL	0.04	0.0246	0.0244	0.0002	0.00057	0.00079
TR-1	LD	0.04	0.0177	0.004	0.0137	0.00041	0.00007
TR-1	HD	0.04	0.0215	0.002	0.0195	0.00007	0.0
TR-1	BL	0.03	0.0248	0.0262	-0.0014	0.00067	0.00083
TR-1	LD	0.03	0.0174	0.005	0.0124	0.00017	0.00047
TR-1	HD	0.03	0.0216	0.0011	0.0205	0.00008	0.00011
TR-1	BL	0.02	0.0269	0.0271	-0.0002	0.00087	0.00044
TR-1	LD	0.02	0.0133	0.013	0.0003	0.00034	0.0001
TR-1	HD	0.02	0.0182	0.0099	0.0008	0.00041	0.00003
TR-1	BL	PFT	0.0367	0.042	-0.0053	0.0031	0.001
TR-1	LD	PFT	0.0425	0.0423	0.0002	0.0043	0.00098
TR-1	HD	PFT	0.0441	0.0389	0.0052	0.0021	0.00082
TR-2	BL	0.04	0.012	0.011	0.001	0.0005	0.00014
TR-2	LD	0.04	0.008	0.001	0.007	0.00002	0.0
TR-2	HD	0.04	0.01	0.0004	0.0096	0.00004	0.00009
TR-2	BL	0.03	0.013	0.014	-0.001	0.00045	0.00067
TR-2	LD	0.03	0.009	0.0003	0.008	0.00003	0.00001
TR-2	HD	0.03	0.009	0.0003	0.009	0.00005	0.00011
TR-2	BL	0.02	0.013	0.015	-0.002	0.00039	0.00032
TR-2	LD	0.02	0.010	0.0016	0.008	0.00062	0.00011
TR-2	HD	0.02	0.011	0.0013	0.010	0.00036	0.00082
TR-2	BL	PFT	0.033	0.032	0.001	0.0012	0.0009
TR-2	LD	PFT	0.031	0.017	0.014	0.0011	0.0014
TR-2	HD	PFT	0.034	0.018	0.016	0.0011	0.0009

All the calculated decay coefficients were plotted versus the water depth for the HD (green), LD (orange) and BL (blue) layouts in Figure 7.3. Overall, the wave decay coefficients for the HD cases were larger than both the LD and BL coefficients which was expected due to the larger quantity of mangrove trunks.

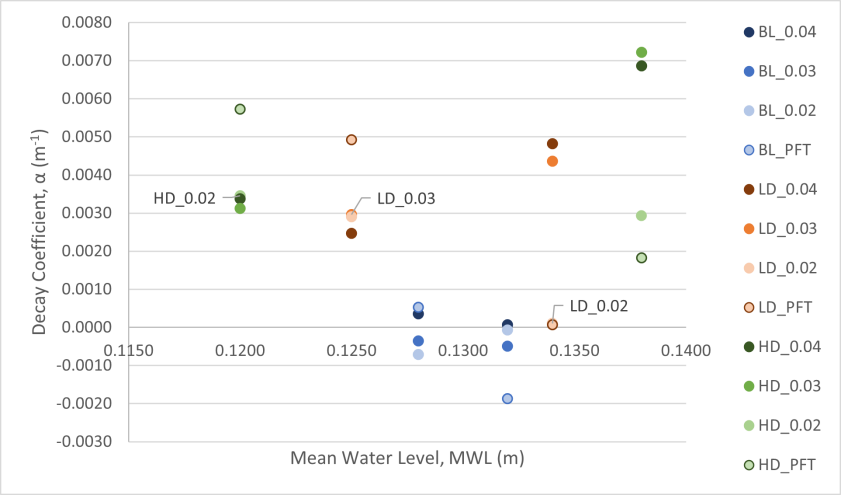

Figure 7.3. Wave Decay coefficients, α, versus the mean water level, MWL, for each trial and layout

Table 7.2 gives the breakdown of the wave decay coefficients for each layout and trial. Once these values were found it became possible to start determining the drag coefficient for each trial and layout using Equation 2.3.

Table 7.2. Summary table of wave height decay, α, for all trials

Mangrove Case	TR-1				TR-2			
	$\alpha_{0.04}$ (m^{-1})	$\alpha_{0.03}$ (m^{-1})	$\alpha_{0.02}$ (m^{-1})	α_{PFT} (m^{-1})	$\alpha_{0.04}$ (m^{-1})	$\alpha_{0.03}$ (m^{-1})	$\alpha_{0.02}$ (m^{-1})	α_{PFT} (m^{-1})
BL	0.0001	-0.0005	-0.0001	-0.0019	0.0004	-0.0004	-0.0007	0.0005
LD	0.0048	0.0044	0.0001	0.0001	0.0025	0.0030	0.0029	0.0049
HD	0.0069	0.0072	0.0029	0.0018	0.0034	0.0031	0.0035	0.0057

7.2. Drag Coefficient

The values for the drag coefficent were calculated using Equation 2.3 from Dalrymple et al. [10]. The incident wave height, H_i, was based on the values collected at the first wave gauge prior to any interaction with the mangrove forest. All the calculated drag coefficients were plotted versus the water depth for the HD (green or yellow) and LD (orange or blue) layouts in Figure 7.4 for both projected area calculations.

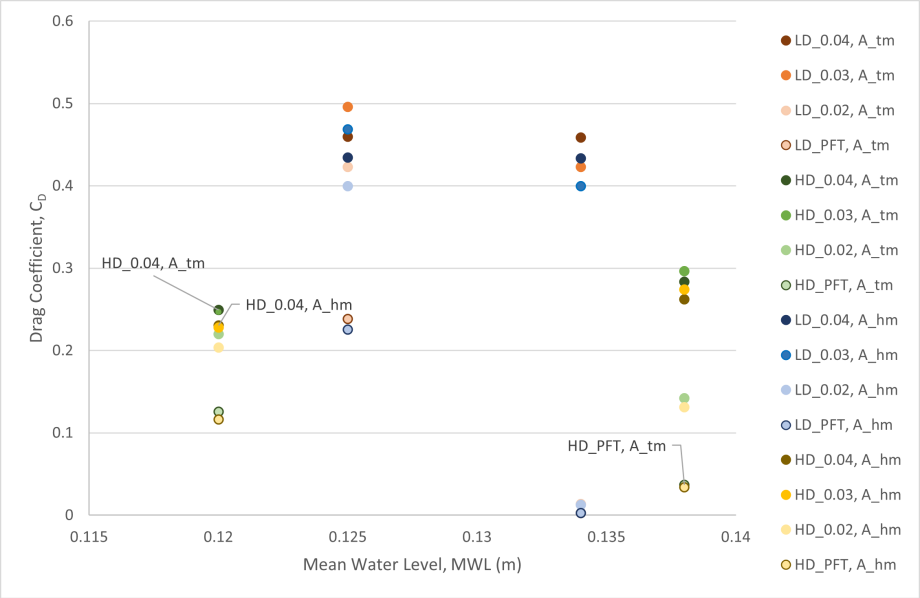

Figure 7.4. Drag Coefficients, C_D, versus the mean water level, MWL, for each trial and layout

Overall, the LD case produced a higher drag coefficient than the HD case which was unexpected and this is believed to have occurred due to the spacing of the trunks in the HD case. Since the trunks that lie directly behind another in the cross-shore direction are only spaced 0.28m apart and the wavelengths vary from 0.63m to 1.35m, it's presumed that there is not enough space for another wave to fully form before reaching the next trunk. This leads to the drag coefficient being less for the HD case than the LD case.

Table 7.3. Summary table of the wave cases with calculated C_D values based on both Projected Areas, $A_{h,m}$ and $A_{t,m}$

Mangrove Case	$A_{h,m}$				$A_{t,m}$			
	$C_{D,0.04}$ (-)	$C_{D,0.03}$ (-)	$C_{D,0.02}$ (-)	$C_{D,PFT}$ (-)	$C_{D,0.04}$ (-)	$C_{D,0.03}$ (-)	$C_{D,0.02}$ (-)	$C_{D,PFT}$ (-)
	TR-1							
LD	0.434	0.400	0.013	0.0026	0.459	0.423	0.013	0.0028
HD	0.262	0.274	0.131	0.034	0.283	0.296	0.142	0.037
	TR-2							
LD	0.434	0.469	0.400	0.225	0.460	0.496	0.423	0.238
HD	0.231	0.228	0.203	0.116	0.249	0.247	0.220	0.126

Chapter 8. Discussion

Table 7.2 shows the overall results for all the trials that were completed for the regular waves. Similarly to Kelty et al. [12], three varying layouts were considered: baseline, low-density, and high-density with the low-density case containing half the mangroves as the high-density case. The baseline case does amplify rather than attenuate, but this could be due to the length of the flume. The flume is only 4.9 m long before reaching the beach slope, due to this limited length there is the possibility that the wave is still developing as it moves through the flume. Since there is no forest in the baseline case, the wave is able to continuously develop as it moves rather than be disrupted like it is in the LD and HD cases. The numerical flume results showed that a higher density mangrove forest yielded the largest wave decay rate. This was expected due to the increased surface area causing drag and minimizing the area for the waves to form throughout the flume. This also validates the numerical flume when compared to previous physical flume experiments as they had the largest wave decay rate for the higher density forest as well. Table 7.2 also shows how the finer mesh causes the numerical results to be closer to the experimental results. The difference between the 0.04 m and 0.03 m meshes produce a similar value for attenuation, but the 0.02 m mesh produces an attenuation value almost identical to the physical experimental value.

However, the drag coefficient results provided a more complicated result. Table 7.3 is a summary of all the drag coefficient results, but when compared to the physical flume results, specifically from Kelty et al. [4], there was a noticeable pattern in the numerical results. The numerical flume produced a larger drag coefficient for the low-density cases than it did for the high-density cases. The low-density drag coefficients ranged from 0.036-

0.496 and the high-density drag coefficients ranged from 0.068-0.296; however, there were a few instances in the previous physical flume experiment where the lower density forest yielded a larger drag coefficient [4]. As previously mentioned in Section 7.2, the reason for the larger drag coefficient may be due to trunk spacing in the flume. Since the trunks that lie directly behind another in the cross-shore direction are only spaced 0.28m apart and the wavelengths vary from 0.63m to 1.35m, it's presumed that there is not enough space for another wave to fully form before reaching the next trunk. This leads to the drag coefficient being less for the HD case than the LD case. However, the two different methods of determining the mean projected area did not seem to have a major effect on the values of the drag coefficient, but the method using the actual projected area per tree per unit height produced smaller results. Overall, the HD case for TR-2 had the best correlation between the numerical and physical results for drag and shown in Figure 7.4.

Chapter 9. Conclusion

This research focused on the creation of a numerical wave flume and studying the effects of mangrove trunks on wave attenuation. The numerical flume was created using Proteus, an open-source Python toolkit, and was based on the bathymetry of the physical wave flume located in PFT which consisted of a flat floor until reaching the beach slope at the end. Two different wave conditions were tested with various wave heights, wave lengths, and water depth as noted in Table 6.1 and each of these trials were run with three varying mangrove forest layouts. The three layouts tested included baseline (no mangroves), low-density, and high density where the high-density layout had double the mangroves as the low-density. Overall, this research was successful in the creation of the numerical flume and it's ability to create waves. The inclusion of the forests demonstrated that a higher density forest produced a higher wave decay rate when directly compared to the wave decay rates produced by the low-density and baseline layouts as visualized in Figure 7.3 in Section 7.1. When the drag coefficient was analyzed, the low-density forest produced higher results than the high-density layout, but this was most likely due to the spacing of the mangrove trunks as previously discussed. The results of the drag coefficients for each trial and layout can be easily compared in Figure 7.4 in Section 7.2.

In conclusion, the objectives of this research were completed; however, there is room for future work. The next possible steps include addition of the prop root systems to the previously embedded mangrove trunks based on the idealized forest implemented by Bryant et al. [8]. In addition, implementation the LiDAR scans of real-world mangrove roots into the numerical flume. All the code for this experiment can be found at https://github.com/rschur3/Rebecca-Thesis/

Appendix A. Mangrove Forest Paraview Visualization

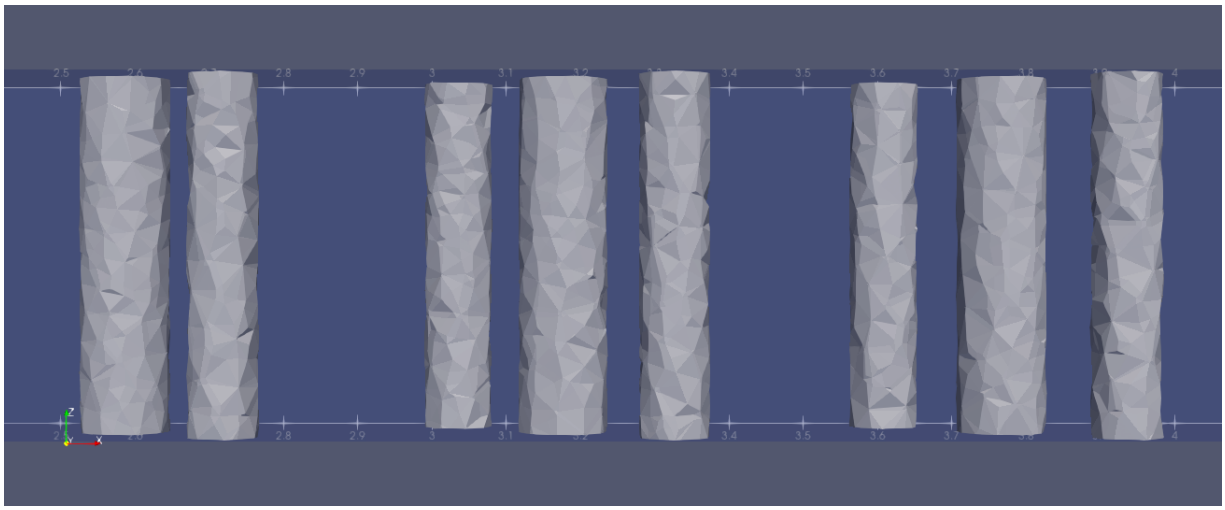

Figure A.1. Side View of LD layout from Paraview

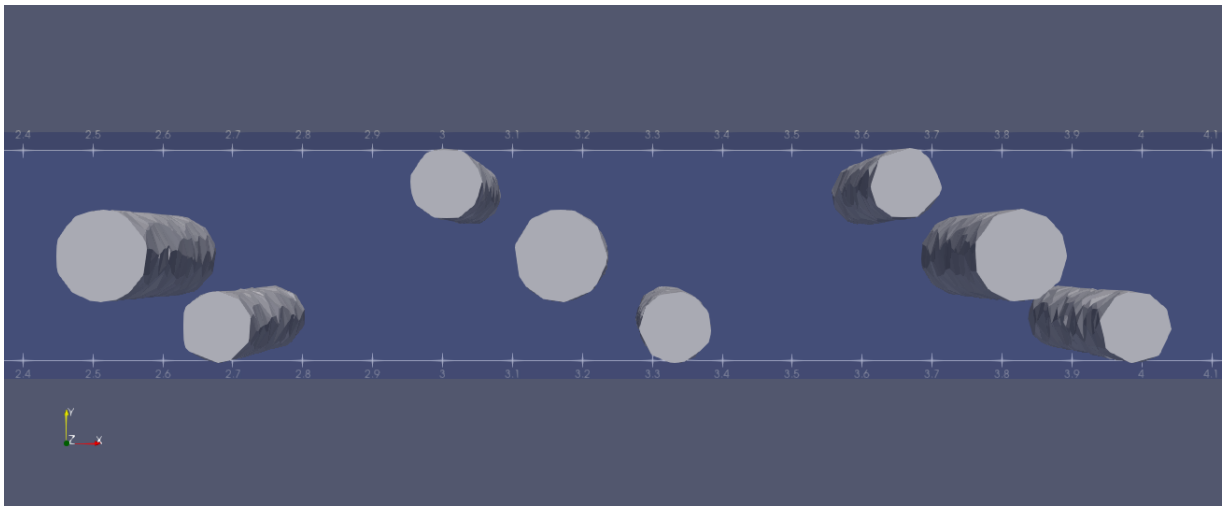

Figure A.2. Top View of LD layout from Paraview

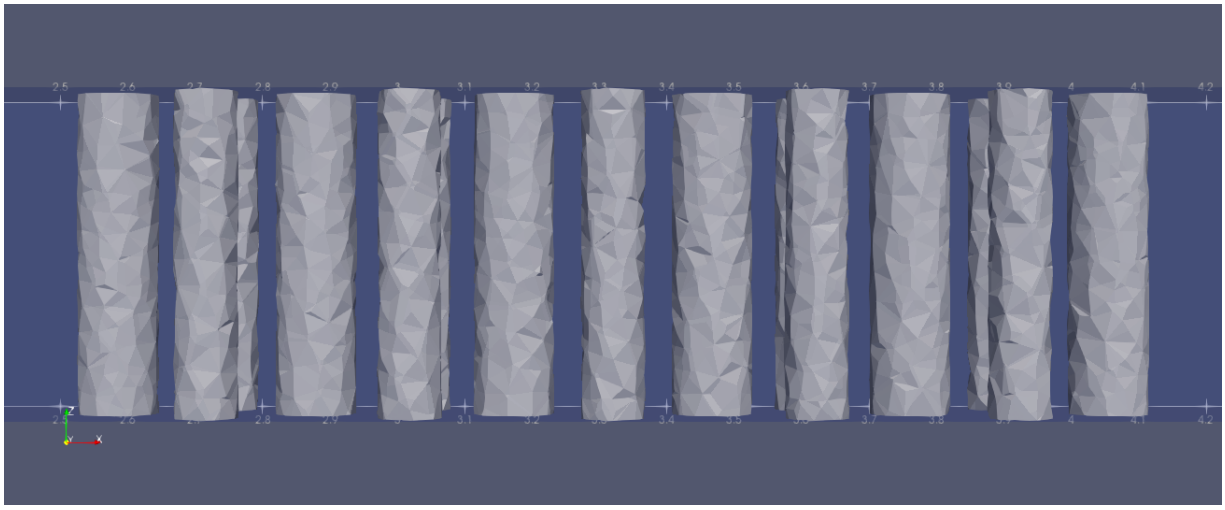

Figure A.3. Side View of HD layout from Paraview

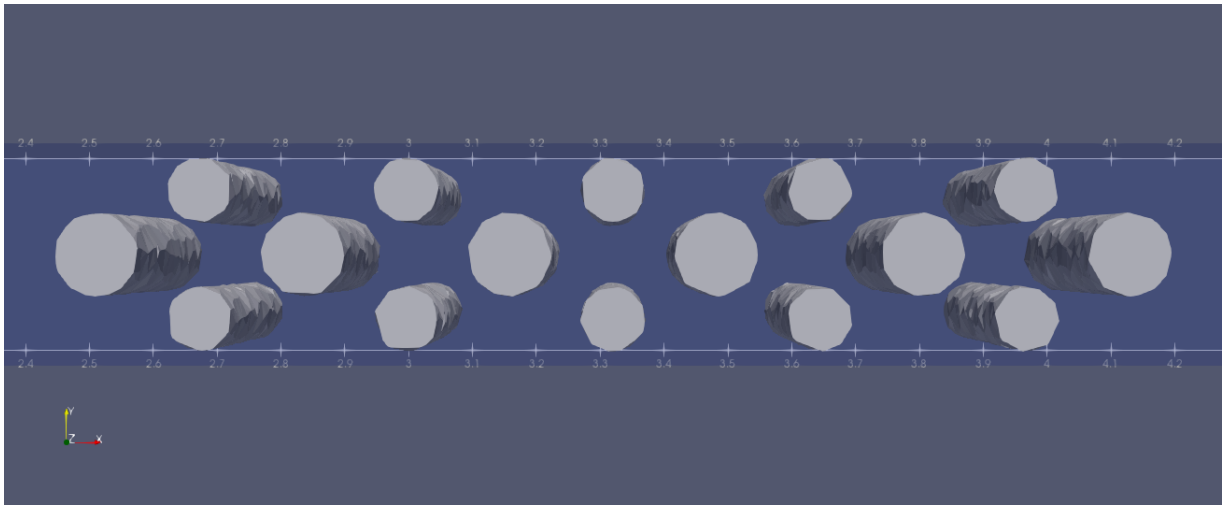

Figure A.4. Top View of HD layout from Paraview

Appendix B. TR-1 Wave Gauge Results

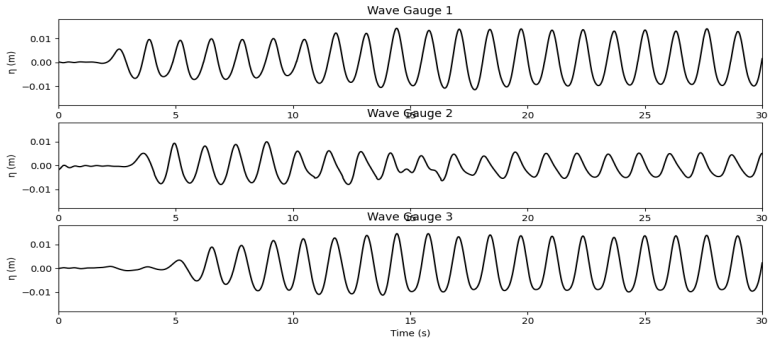

Figure B.1. WG Results for Numerical Flume for TR-1 BL Case for he=0.04m

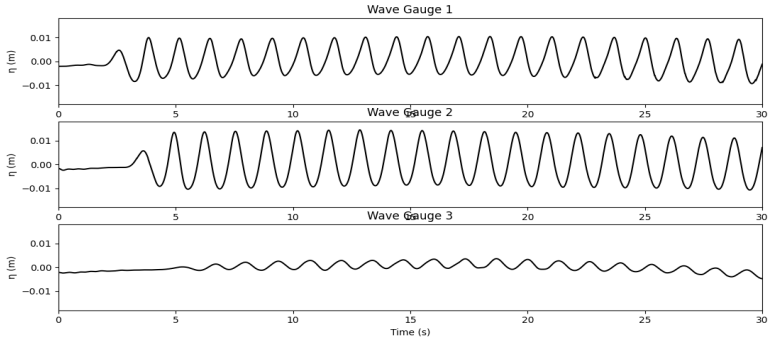

Figure B.2. WG Results for Numerical Flume for TR-1 LD Case for he=0.04m

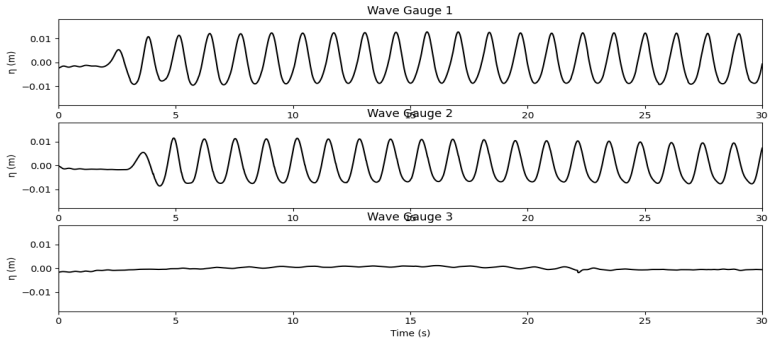

Figure B.3. WG Results for Numerical Flume for TR-1 HD Case for he=0.04m

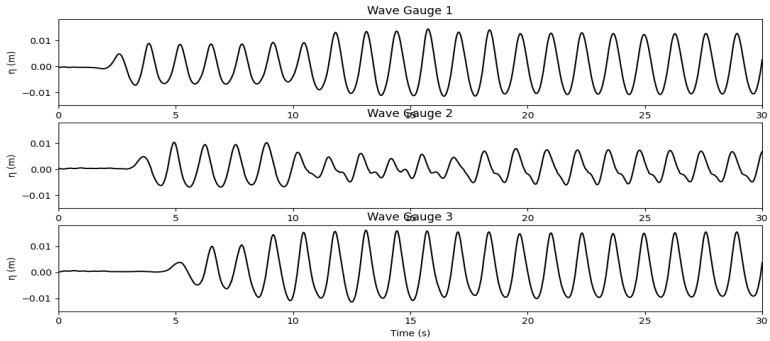

Figure B.4. WG Results for Numerical Flume for TR-1 BL Case for he=0.03m

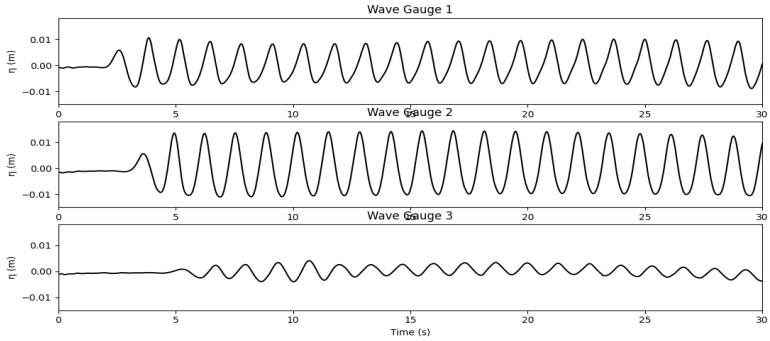

Figure B.5. WG Results for Numerical Flume for TR-1 LD Case for he=0.03m

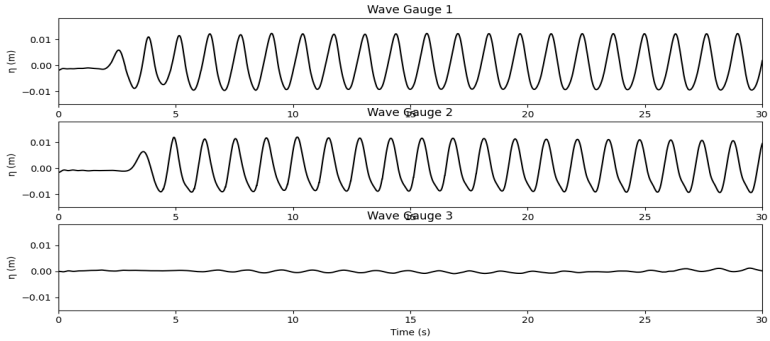

Figure B.6. WG Results for Numerical Flume for TR-1 HD Case for he=0.03m

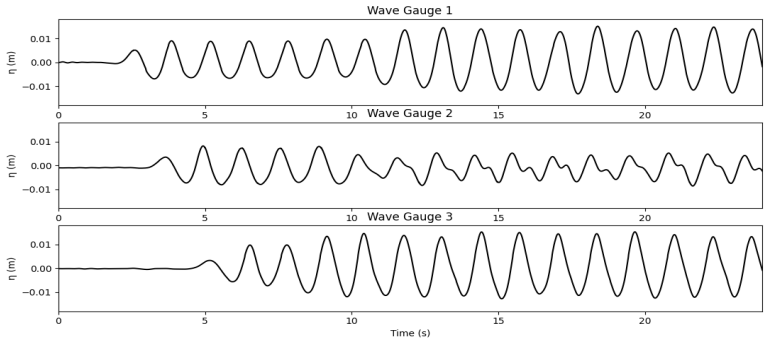

Figure B.7. WG Results for Numerical Flume for TR-1 BL Case for he=0.02m

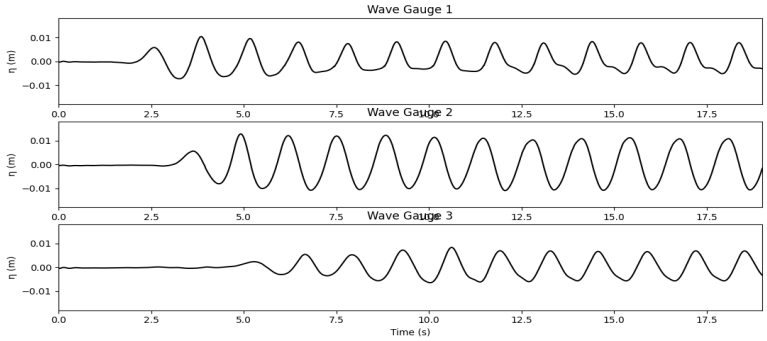

Figure B.8. WG Results for Numerical Flume for TR-1 LD Case for he=0.02m

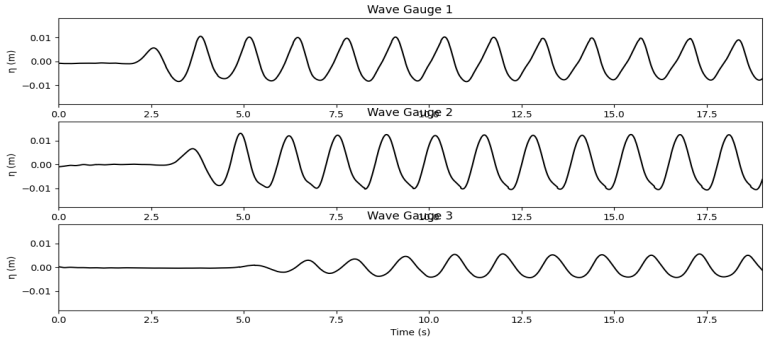

Figure B.9. WG Results for Numerical Flume for TR-1 HD Case for he=0.02m

Appendix C. TR-2 Wave Gauge Results

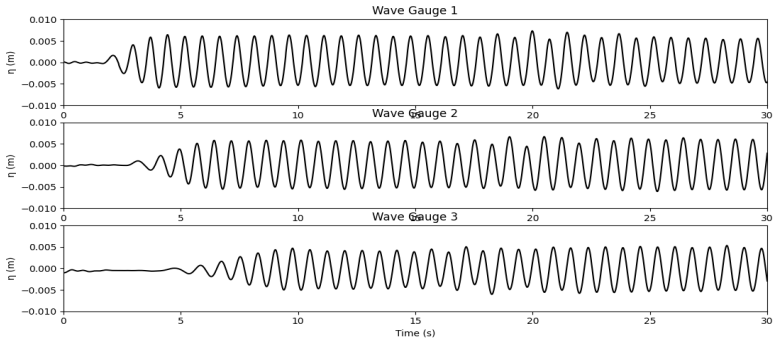

Figure C.1. WG Results for Numerical Flume for TR-2 BL Case for he=0.04m

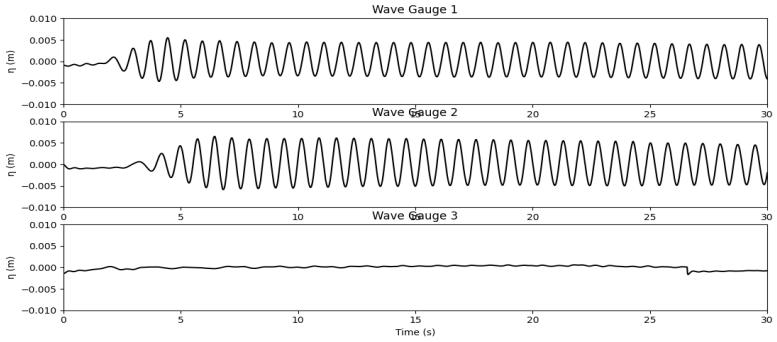

Figure C.2. WG Results for Numerical Flume for TR-2 LD Case for he=0.04m

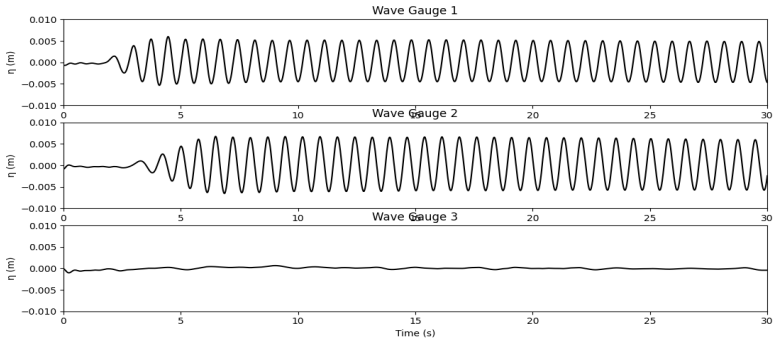

Figure C.3. WG Results for Numerical Flume for TR-2 HD Case for he=0.04m

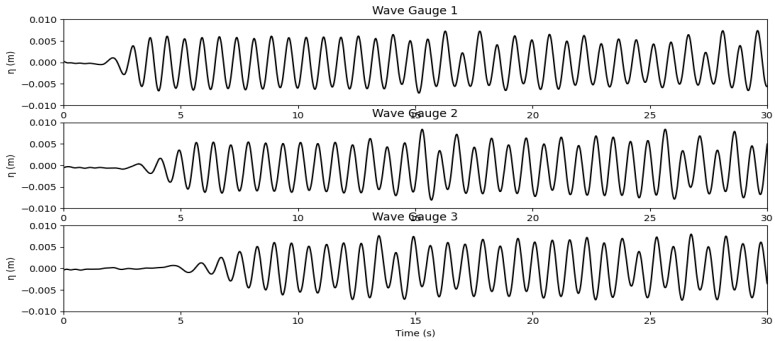

Figure C.4. WG Results for Numerical Flume for TR-2 BL Case for he=0.03m

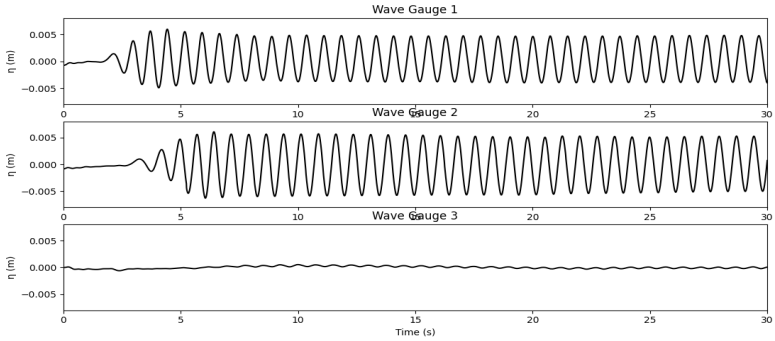

Figure C.5. WG Results for Numerical Flume for TR-2 LD Case for he=0.03m

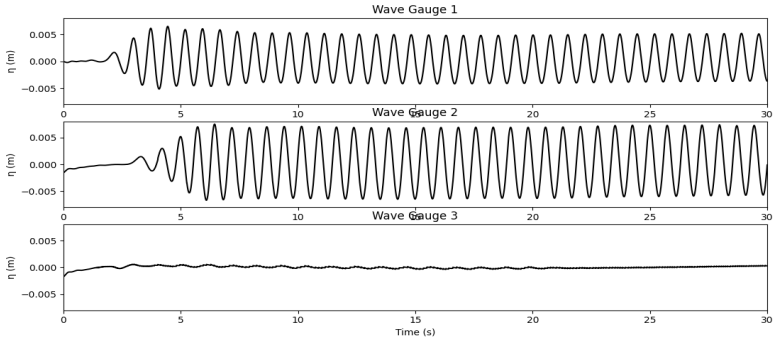

Figure C.6. WG Results for Numerical Flume for TR-2 HD Case for he=0.03m

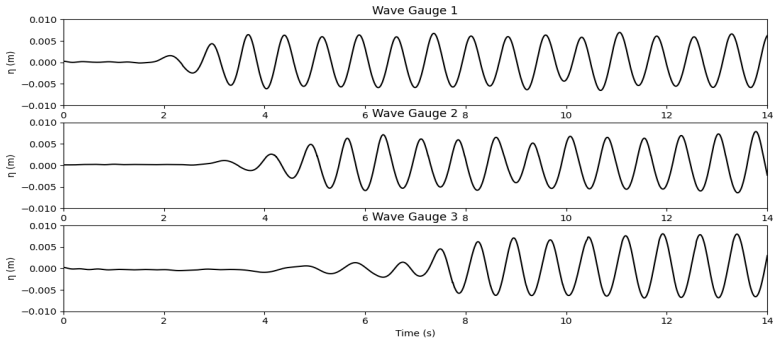

Figure C.7. WG Results for Numerical Flume for TR-2 BL Case for he=0.02m

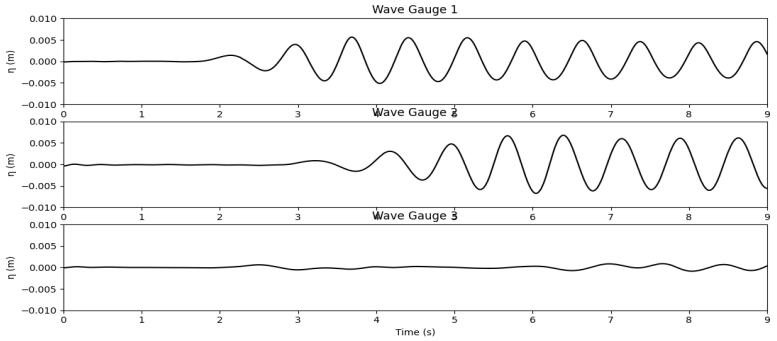

Figure C.8. WG Results for Numerical Flume for TR-2 LD Case for he=0.02m

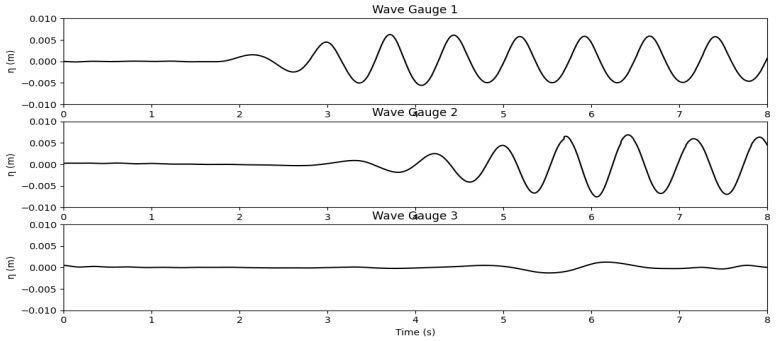

Figure C.9. WG Results for Numerical Flume for TR-2 HD Case for he=0.02m

Appendix D. Projected Area Bays

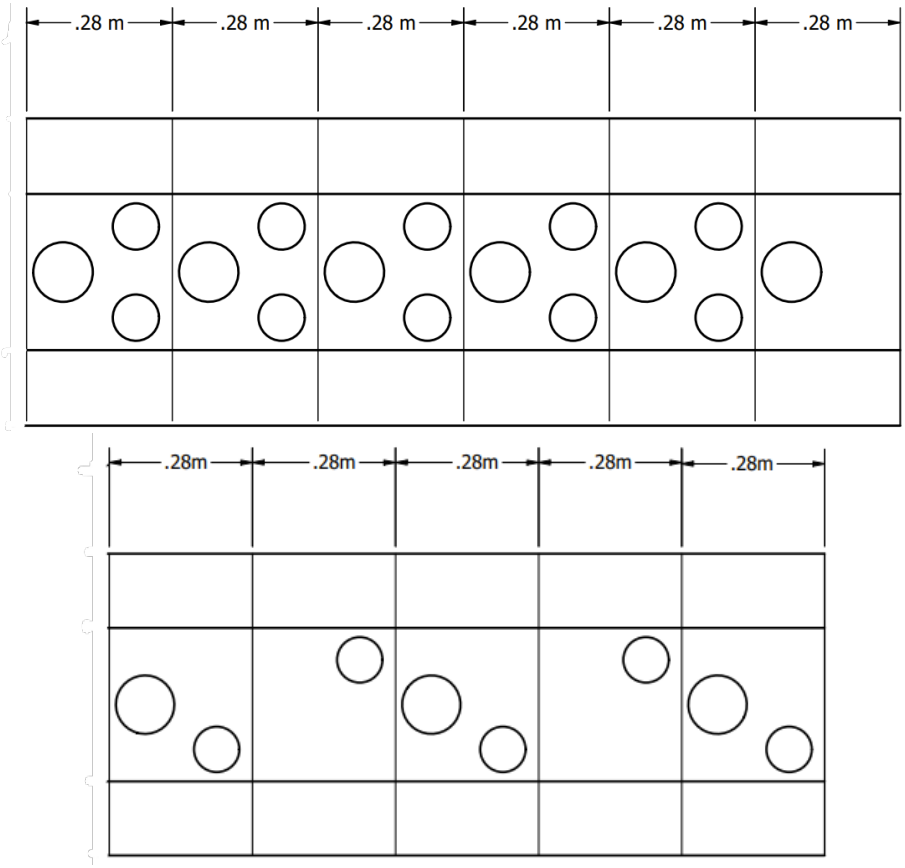

Figure D.1. Mangrove forest section bay divison for HD (upper) and LD (lower) cases

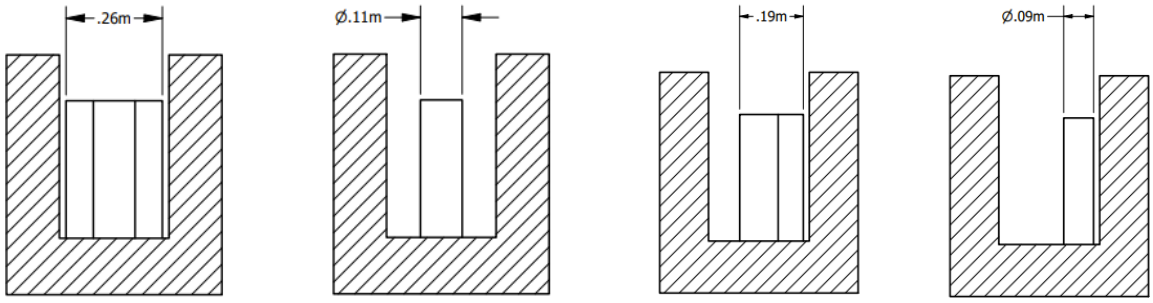

Figure D.2. Cross-sectional schematic of bays for HD and LD cases

Appendix E. Wave Decay Rates Results

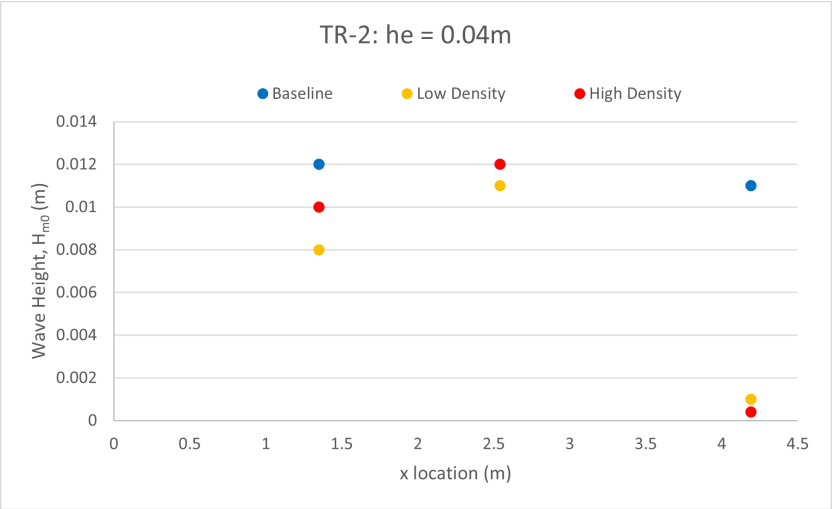

Figure E.1. Total spectral estimate of the significant wave height, H_s, with respect to x location for wave gauges for TR-2 with he=0.04m

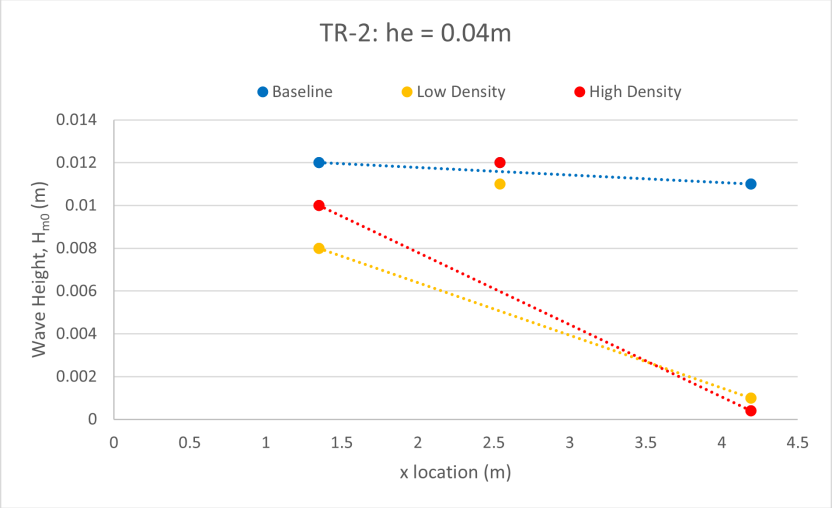

Figure E.2. Total spectral estimate of the significant wave height, H_s, and linear line of best fit for each layout for TR-2 with he=0.04m

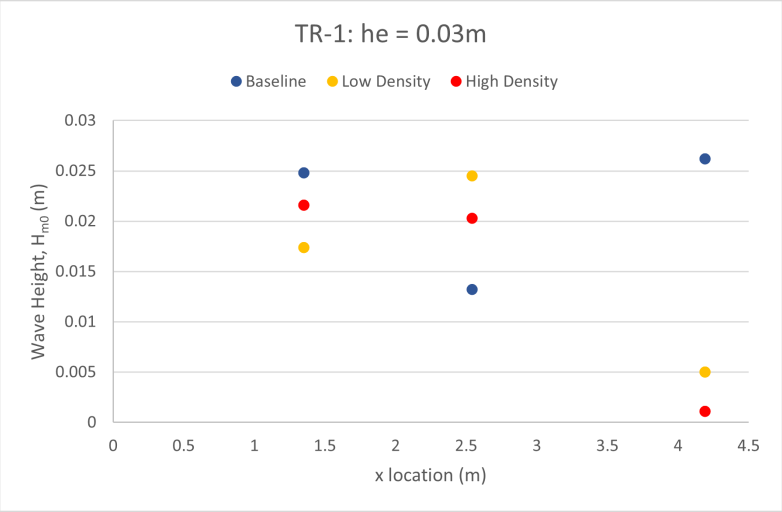

Figure E.3. Total spectral estimate of the significant wave height, H_s, with respect to x location for wave gauges for TR-1 with he=0.03m

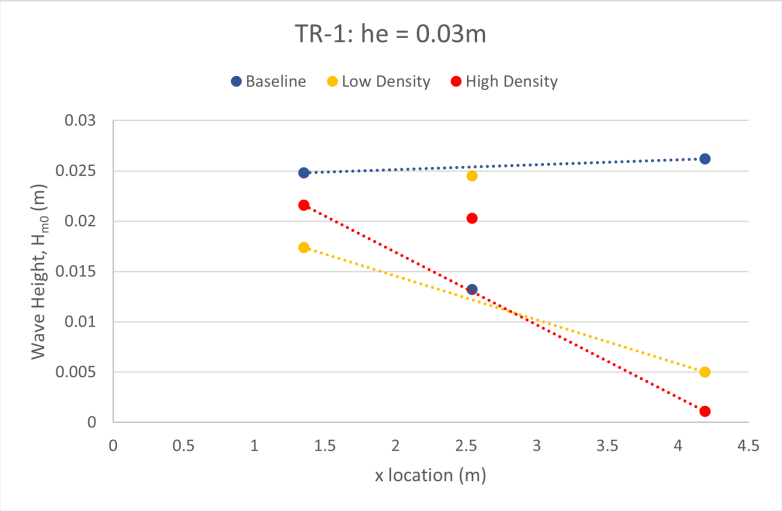

Figure E.4. Total spectral estimate of the significant wave height, H_s, and linear line of best fit for each layout for TR-1 with he=0.03m

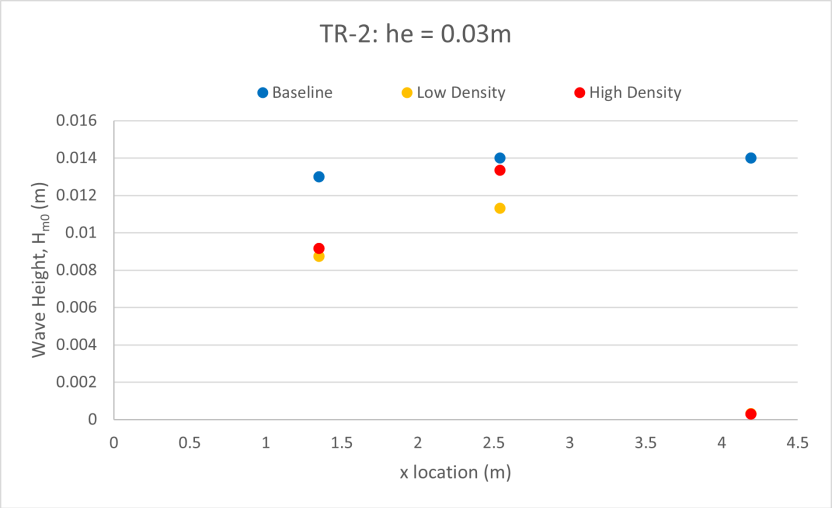

Figure E.5. Total spectral estimate of the significant wave height, H_s, with respect to x location for wave gauges for TR-2 with he=0.03m

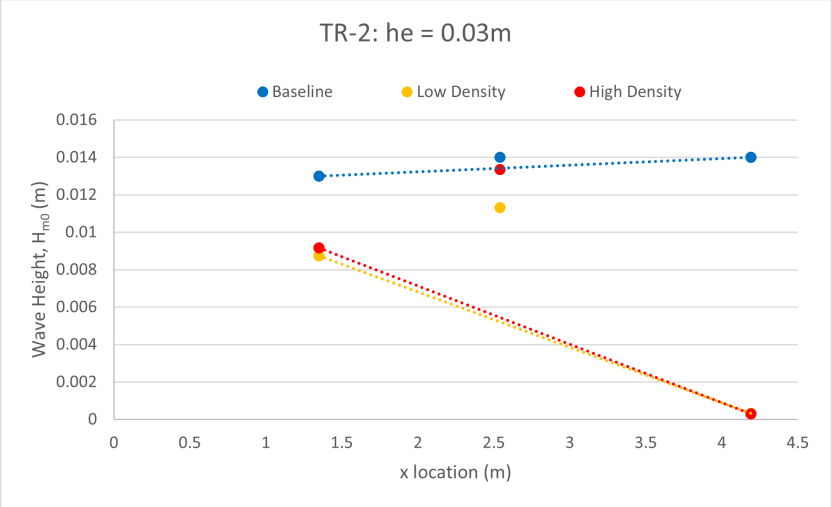

Figure E.6. Total spectral estimate of the significant wave height, H_s, and linear line of best fit for each layout for TR-2 with he=0.03m

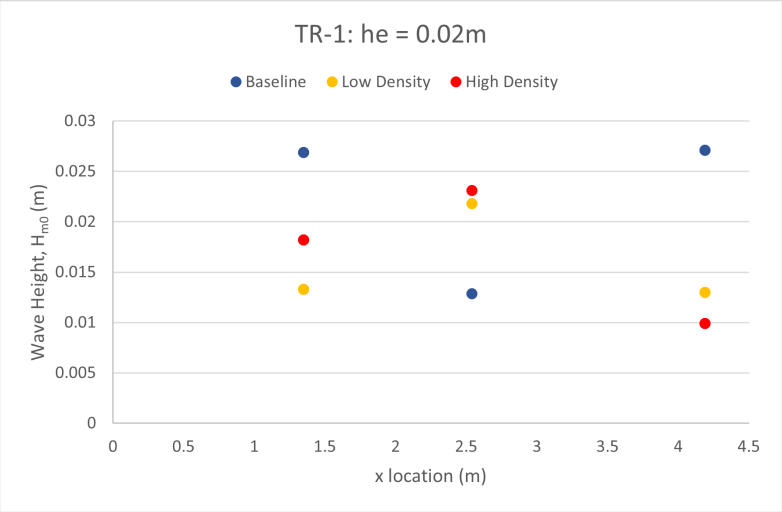

Figure E.7. Total spectral estimate of the significant wave height, H_s, with respect to x location for wave gauges for TR-1 with he=0.02m

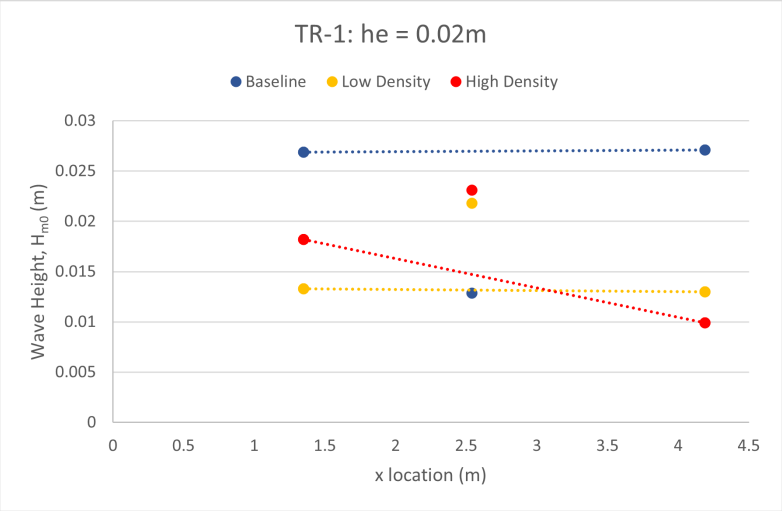

Figure E.8. Total spectral estimate of the significant wave height, H_s, and linear line of best fit for each layout for TR-1 with he=0.02m

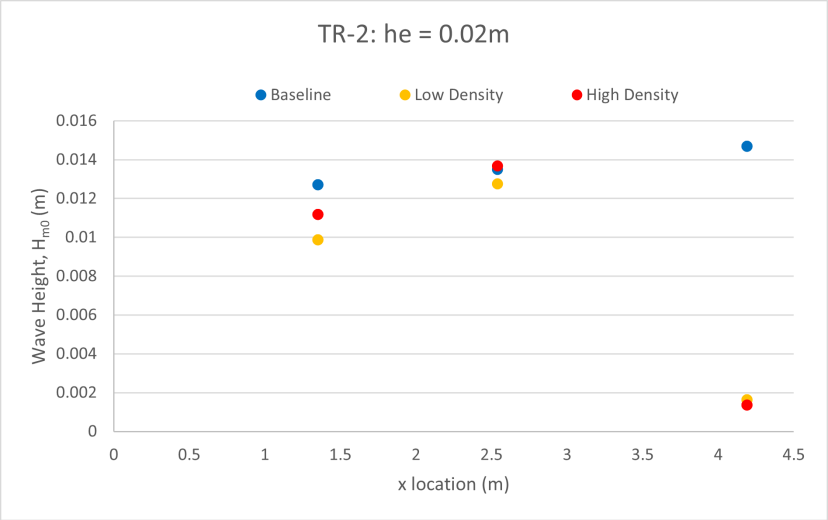

Figure E.9. Total spectral estimate of the significant wave height, H_s, with respect to x location for wave gauges for TR-2 with he=0.02m

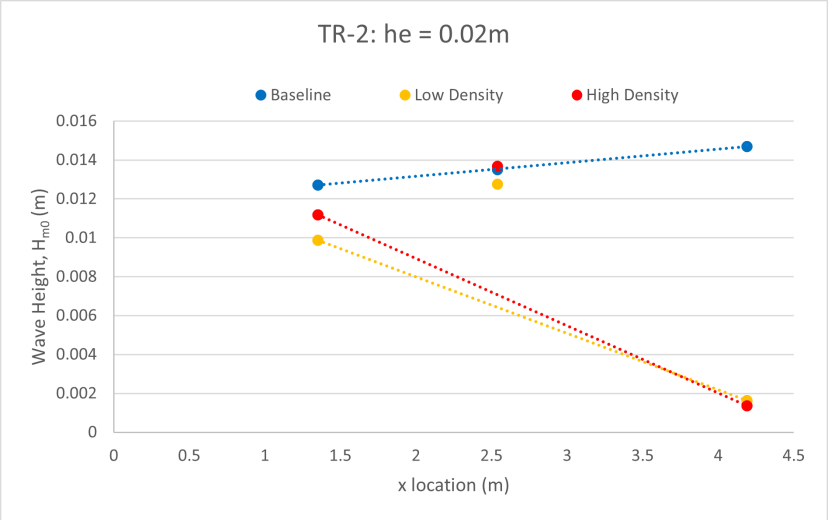

Figure E.10. Total spectral estimate of the significant wave height, H_s, and linear line of best fit for each layout for TR-2 with he=0.02m

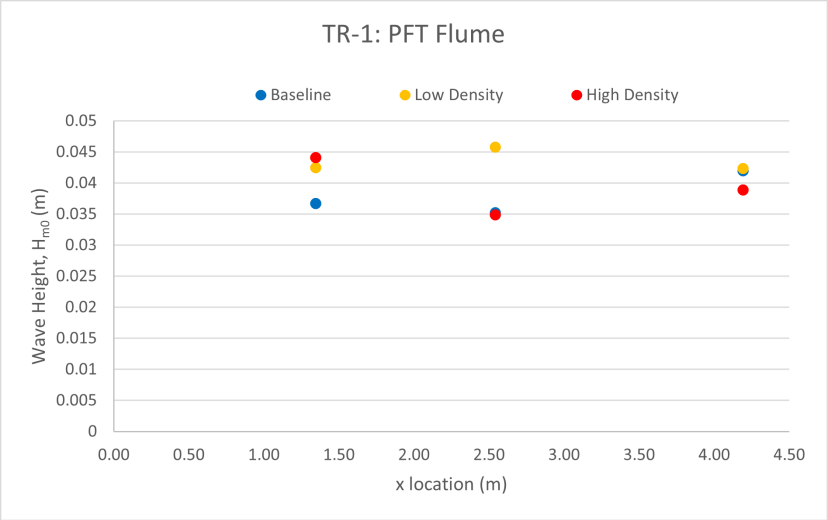

Figure E.11. Total spectral estimate of the significant wave height, H_s, with respect to x location for wave gauges for PFT TR-1

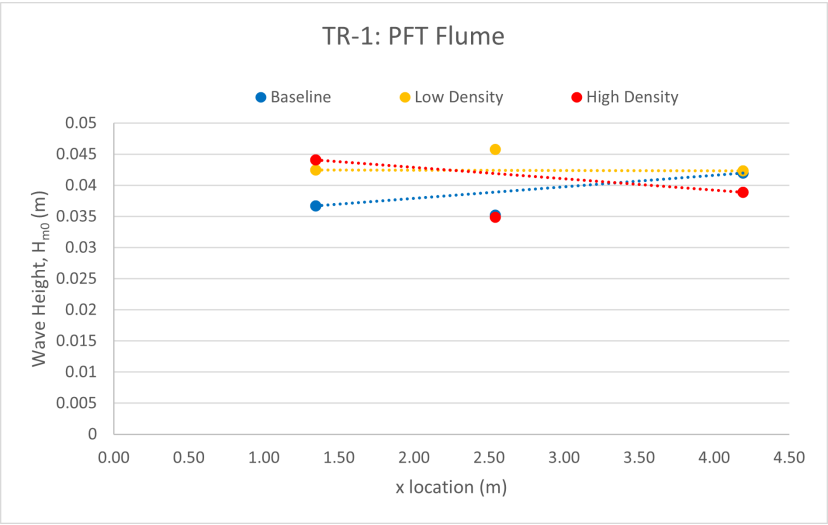

Figure E.12. Total spectral estimate of the significant wave height, H_s, and linear line of best fit for each layout for PFT TR-1

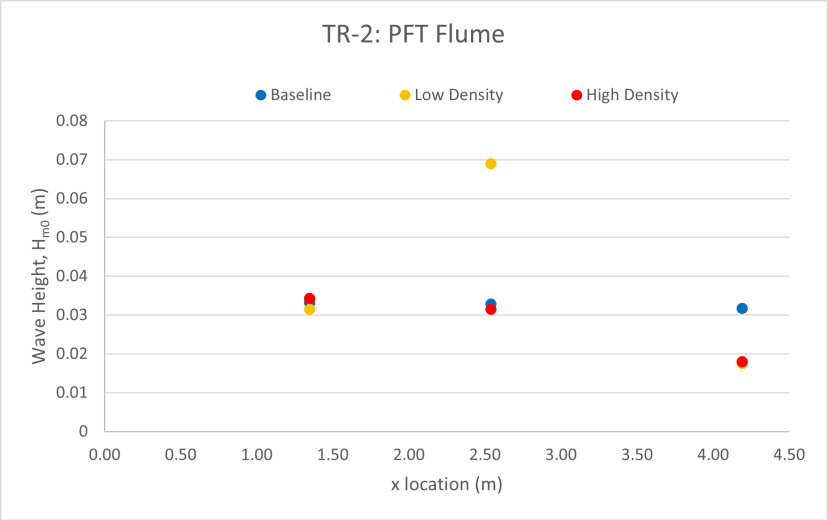

Figure E.13. Total spectral estimate of the significant wave height, H_s, with respect to x location for wave gauges for PFT TR-2

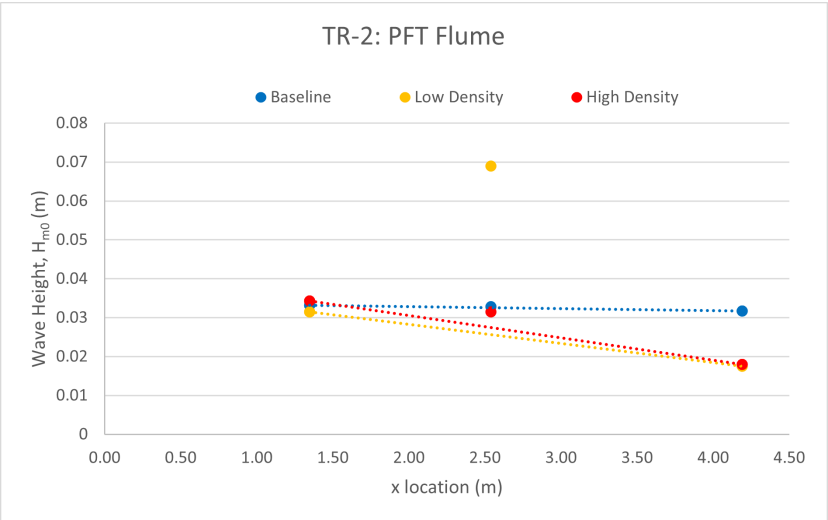

Figure E.14. Total spectral estimate of the significant wave height, H_s, and linear line of best fit for each layout for PFT TR-2

Bibliography

[1] Xiaofeng Zhang, Vivien P. Chua, and Hin-Fatt Cheong. Hydrodynamics in mangrove prop roots and their physical properties. *Journal of Hydro-environment Research*, 9(2):281–294, June 2015.

[2] Maria Maza, Katherine Adler, Diogo Ramos, Adrian Mikhail Garcia, and Heidi Nepf. Velocity and Drag Evolution From the Leading Edge of a Model Mangrove Forest. *Journal of Geophysical Research: Oceans*, 122(11):9144–9159, 2017. _eprint: https://onlinelibrary.wiley.com/doi/pdf/10.1002/2017JC012945.

[3] Maria Maza, Javier L. Lara, and Iñigo J. Losada. Experimental analysis of wave attenuation and drag forces in a realistic fringe Rhizophora mangrove forest. *Advances in Water Resources*, 131:103376, September 2019.

[4] Kiernan Kelty. Prototype-scale physical model study of wave attenuation by an idealized mangrove forest of moderate cross-shore width. Master's thesis, Oregon State University, 2021.

[5] Anita Hansbo and Peter Hansbo. An unfitted finite element method, based on NitscheÕs method, for elliptic interface problems. *Comput. Methods Appl. Mech. Engrg.*, page 16, 2002.

[6] Erik Burman, Susanne Claus, Peter Hansbo, Mats G. Larson, and André Massing. CutFEM: Discretizing geometry and partial differential equations. *International Journal for Numerical Methods in Engineering*, 104(7):472–501, November 2015.

[7] Christopher E. Kees, J. Haydel Collins, and Alvin Zhang. Simple, accurate, and efficient embedded finite element methods for fluid–solid interaction. *Computer Methods in Applied Mechanics and Engineering*, 389:114404, February 2022.

[8] Mary Anderson Bryant, Duncan B Bryant, Leigh A Provost, Nia Hurst, Maya McHugh, Anna Wargula, and Tori Tomiczek. Wave Attenuation of Coastal Mangroves at a Near-Prototype Scale. *Engineer Research and Development Center*, page 126, September 2022.

[9] National Research Council (U.S.). Panel on Wave Action Effects Associated with Storm Surges. *Methodology for Calculating Wave Action Effects Associated with Storm Surges*. National Academy of Sciences, 1977.

[10] Robert A. Dalrymple, James T. Kirby, and Paul A. Hwang. Wave Diffraction Due to Areas of Energy Dissipation. *Journal of Waterway, Port, Coastal, and Ocean Engineering*, 110(1):67–79, February 1984.

[11] Fernando J. Mendez and Inigo J. Losada. An empirical model to estimate the prop-

agation of random breaking and nonbreaking waves over vegetation fields. *Coastal Engineering*, 51(2):103–118, April 2004.

[12] Kiernan Kelty, Tori Tomiczek, Daniel Thomas Cox, Pedro Lomonaco, and William Mitchell. Prototype-Scale Physical Model of Wave Attenuation Through a Mangrove Forest of Moderate Cross-Shore Thickness: LiDAR-Based Characterization and Reynolds Scaling for Engineering With Nature. *Frontiers in Marine Science*, 8, 2022.

[13] Aggelos S. Dimakopoulos, Tristan de Lataillade, and Chris E. Kees. Fast random wave generation in numerical tanks. *Proceedings of the Institution of Civil Engineers - Engineering and Computational Mechanics*, pages 1–29, April 2019.

[14] Kiernan Kelty, Daniel Cox, Tori Tomiczek, and Pedro Lomonaco. Experimental investigation of wave, surge, and tsunami transformation over natural shorelines, Sep 2021. Type: dataset.

[15] Andre S. Rovai, Robert R. Twilley, Edward Castañeda-Moya, Stephen R. Midway, Daniel A. Friess, Carl C. Trettin, Jacob J. Bukoski, Atticus E.L. Stovall, Paulo R. Pagliosa, Alessandra L. Fonseca, Richard A. Mackenzie, Aslan Aslan, Sigit D. Sasmito, Mériadec Sillanpää, Thomas G. Cole, Joko Purbopuspito, Matthew W. Warren, Daniel Murdiyarso, Wolfram Mofu, Sahadev Sharma, Pham Hong Tinh, and Pablo Riul. Macroecological patterns of forest structure and allometric scaling in mangrove forests. *Global Ecology and Biogeography*, 30(5):1000–1013, 2021.

Vita

Rebecca Schurr grew up in Pennsylvania and received her bachelor degree in Environmental Engineering from the University of Delaware in 2021. Afterwards, she moved to Louisiana to study Coastal and Ecological Engineering at the Louisiana State University. She plans to receive her master's degree in May of 2023.